Eigenmodes of the quasi-periodic one-dimensional wire

E. Akkermans and E. Gurevich
Technion
(Dated: April 26, 2014)

The eigenmodes of the quasi-periodic one-dimensional system are calculated and visualized as an intensity map in the position-energy axes. The spectral function $a(E,k)$ is calculated as well and visualized as an intensity map in the momentum-energy axes. The calculated figures look very similar to the experimental observation. For the final conclusion, however, we need to know more precisely the experimental parameters describing the system.

Contents

I. BRIEF DESCRIPTION OF THE CONSIDERED SYSTEM

The considered sample is a quasi one-dimensional (1D) exciton-polariton wire with a quasi-periodically modulated width. It consists in a high quality factor $\lambda/2$ vertical (z-axis) planar cavity containing GaAs quantum wells in the anti-node horizontal plane. In the horizontal $x-y$ plane the cavity is shaped into a quasi-1D structure, a wire, of the length of 200 μm and quasi-periodically modulated width of a few μm (the wire fabrication is by using electron beam lithography and reactive ion etching).

Vertical confinement is much smaller than that in the xy plane for both excitons and photons, which therefore can be considered as 2D objects. The exciton energy E_x and the lowest photonic mode energy E_c are chosen so that the detuning $\delta(0) = E_c - E_x$ is comparable to their coupling Ω. Therefore, excitons and photons are strongly coupled and form polaritons.

The quasiperiodic modulation of the width of the wire is shown schematically in Fig. 1(a). It consists of two elements ("letters") B and A of the same pitch $a = 1.35\,\mu$m and different widths of 2.04 μm and 3.5 μm respectively. The letters are arranged in the quasi-periodic order according to the Fibonacci sequence, constructed using the recursion rule

$$S_{j\geq 3} = [S_{j-2}S_{j-1}]\,, \text{ and } S_1 = B,\ S_2 = A, \tag{1}$$

where $[S_{j-2}S_{j-1}]$ means concatenation of two sub-sequences S_{j-2} and S_{j-1}. Number of the letters in a sequence S_j is given by the Fibonacci number F_j. Here definition of the index of S_j matches the following definition of the Fibonacci numbers $F_0 = 0$, $F_1 = 1$, $F_2 = 1$, $F_3 = 2$ (seemingly, this is the standard convention).

The experimental sample was constructed as a concatenation $[S_1, S_2, ..., S_{10}]$, which turns out to be identical to the sequence S_{12} with the first letter A removed (see Appendix A). In addition, the quasiperiodic part, counting 143 letters, is padded on both sides with nearly 7 A-letters, so that the experimental configuration is

$$\underbrace{AAAAAAA}_{\sim 7 \text{ letters}}\underbrace{S_1 S_2 \cdots S_{10}}_{143 \text{ letters}}\underbrace{AAAAAAA}_{\sim 7 \text{ letters}}, \tag{2}$$

which has a total length of 210 μm. The micrograph of the wire is shown in Fig. 1(b). Modulation of the wire width induces an effective 1D potential for the longitudinal motion of the polaritons, as discussed in the sequel. Thus, as a consequence of the quasi-periodic potential, we expect to observe self-similar features in the spectral properties of the system, as described below. The current theoretical task is to calculate the polaritonic spectrum and compare the result to the experiment.

II. THEORETICAL BACKGROUND

A. Exciton-photon coupling

In a 3D-, 2D or 1D-uniform extended system only the excitons and the photons of the same momentum are coupled, - due to the momentum conservation (either linear or angular). For example, in a uniform quasi-1D wire, it is the momentum along the wire which should be the same, while the transverse and the vertical degrees of freedom are

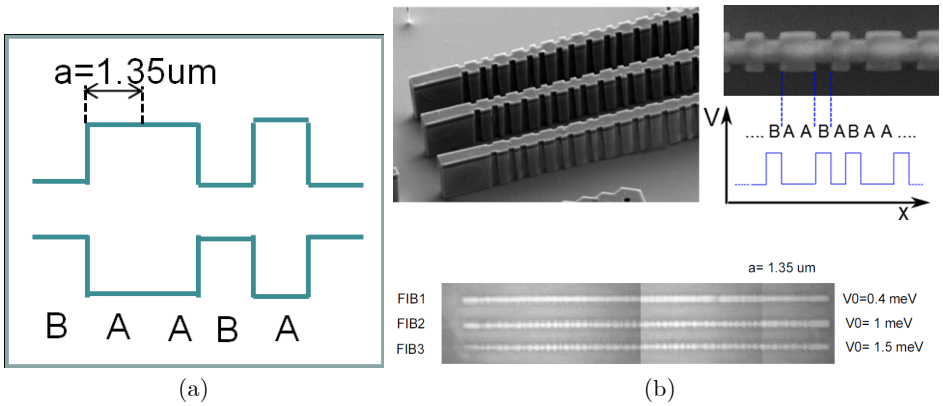

FIG. 1: (a) Schematic presentation of the wire width modulation. (b) Micrographs of the wires.

discrete and are assumed to be fixed. Thus, considering only the longitudinal degree of freedom, a given polaritonic state can be labeled by the momentum of the corresponding coupled exciton and photon. The polaritonic energy is found by the diagonalization of the 2×2 matrix, and is given by the known expression (Hopfield)

$$E_{LP}(k) = E_X + \frac{1}{2}\left(\delta(k) - \sqrt{\delta^2(k) + \Omega_R^2}\right), \tag{3}$$

$$E_{UP}(k) = E_X - \frac{1}{2}\left(\delta(k) - \sqrt{\delta^2(k) + \Omega_R^2}\right), \tag{4}$$

for the lower (LP) and the upper (UP) polaritons, where k is the wave vector and the cavity-exciton detuning $\delta(k) = E_C(k) - E_X$ is a difference between the photonic and excitonic energies (E_X is nearly k-independent). Thus, even if $E_C(k)$ and $E_X(k)$ are parabolic, the polaritonic dispersion is not.

In the considered system, exctitons and photons experience different vertical confinement along z-axis, a thin quantum well and a λ-cavity respectively, while same confinement in the longitudinal (x) and the transverse (y) directions. In both cases, however, the vertical confinement, is much tighter than the lateral one and is uniform over the cavity. Therefore, the vertical degree of freedom is nearly separated from the other two (nearly, - because BCs are not exactly zero). We consider only the lowest vertical mode, both for the excitons and the photons, so that the problem reduces to 2D in xy-plane.

Due to the complex (quasi-periodic) lateral confinement, motion in the xy-plane is not translationally invariant and even not separable. Therefore, the polaritonic eigenstates are not momentum states. If we assume zero boundary conditions on the boundary of the xy domain, then, up to the different mass, the problem is identical for the photons and the excitons. Then the polaritonic spectrum and states can be found in one of the following ways:

1. Similarly to the uniform system, first find separately the eigenstates and the eigenenergies for the photons and the excitons, then couple them. This approach can be used in any case, including different potential/confinement for the photons and the excitons (then all the excitonic states are coupled to all the photonic ones, which is not pleasant). In our case, by the assumption of same BCs, the photon and the center-of-the-mass exciton eigenfunctions would have an identical spatial variation. Therefore, the exciton-photon coupling matrix element (which is proportional to the scalar product of the two) would connect only the states with the same indices (since the eigenfunctions are orthogonal). Then, the polaritonic energies would be given by the expression similar to (3,4), with the wave vector k replaced by the proper quantum number of the original photon or exciton eigenstate. This approach was used, for example, in Ref. [2] for the polaritons in the cylindrical cavity.

2. Alternatively, one can first obtain an effective equation for the polariton and, then, solve it for the spectrum and the states. This approach is practical if the photons and the excitons have an identical confinement and an identical (or zero) potential (otherwise the polaritonic potential/confinement should be something complicated, even if possible to obtain). The simplest way to obtain an equation for the polariton seems to go into the second quantization in the momentum representation, where the kinetic plus the interaction term of the Hamiltonian is diagonal in k and can be completely diagonalized by the Hopfield (Bogolubov?) transformation resulting in (3,4). The latter transformation keeps the same functional form for the non-diagonal in k term, resulting from the lateral confinement[1] (for the details see Appendix [**not written yet**]). Therefore, going back to the position representation, one obtains the same lateral confinement, while the kinetic term would be given by

$$E_{LP/UP}(p/\hbar), \tag{5}$$

where p is the momentum operator and $E_{LP/UP}(k)$ are defined in (3,4).

If $E_{LP/UP}(p/\hbar)$ in (5) is approximated by the parabola, then the two approaches become technically identical. Otherwise, however, they are quite different, and the first one is more convenient for our purposes of the reduction of the 2D problem to the effective 1D problem (see below). This is because the kinetic terms have the simple quadratic form. Thus, in the following we stick to the first approach.

---

[1] The lateral confinement can be introduced by defining zero potential in the outer region and large but finite negative potential, $-|U|$, in the internal one. Then, matrix elements due to the confinement are U times some functions of k and k', same for the photons and the excitons if same U was chosen for both (otherwise it would be k-dependent because of the Hopfield coefficient).

B. Schrodinger-like equation for the 2D photons

The vertical (z) confinement of the photons is realized by two Bragg mirrors. In the lateral dimension, an approximation of zero boundary conditions is used, justified by high dielectric to air contrast of the refractive index. Assuming semi-infinite Bragg mirrors, the problem becomes that of an infinite cylinder in z-direction. Under the above assumptions (IT SEEMS) that the solutions can be chosen to have TE or TM polarizations. Then, for the TE polarization ($\mathcal{E}_z = 0$), the solution can be written with the lateral and z-coordinate separated. For the TM polarization, the situation can be slightly more complicated (because $\nabla \overrightarrow{\mathcal{E}} \neq \mathbf{0}$ at the interfaces, so that $\nabla \times \nabla \times \overrightarrow{\mathcal{E}} \neq -\triangle \overrightarrow{\mathcal{E}}$). Anyway, as a further approximation, the Bragg mirror cavity can be described by a Fabry-Perot planar cavity with some effective refraction index. Then, for any polarization, eigenmode solutions are separable in respect to the lateral xy and vertical z coordinates. Besides, inside the effective cavity with the uniform refraction index $\nabla \overrightarrow{\mathcal{E}} = \mathbf{0}$, and the stationary wave equation reduces to the simplest form

$$\frac{n^2}{c^2}\omega^2 \overrightarrow{\mathcal{E}} = -\triangle \overrightarrow{\mathcal{E}}. \tag{6}$$

Assuming same z-dependence for each component of $\mathbf{E}$, and denoting

$$-\partial_z^2 \overrightarrow{\mathcal{E}} = k_z^2 \overrightarrow{\mathcal{E}}, \tag{7}$$

where $\frac{c}{n}\hbar k_z \equiv E_c$, one obtains the following 2D equation ($\triangle_\perp \equiv \partial_x^2 + \partial_y^2$)

$$\left(\frac{n^2}{c^2}\omega^2 - k_z^2\right) \overrightarrow{\mathcal{E}} = -\triangle_\perp \overrightarrow{\mathcal{E}}. \tag{8}$$

Furthermore, this vector equation is (approximately) replaced by a scalar one (and the condition $\nabla \overrightarrow{\mathcal{E}} = \mathbf{0}$ is still OK due to the form of the exact vector solution either for TE or TM polarizations - this point is still to be cleared out):

$$E\psi(x,y) = -\triangle_\perp \psi(x,y), \tag{9}$$

where by definition

$$E \equiv \frac{n^2}{c^2}\omega^2 - k_z^2 \tag{10}$$

(i.e. E has an inverse dimension of the length squared), and $\psi(x,y)$ satisfies zero BC on the lateral boundary.

Since the vertical confinement is much tighter than the lateral one, in the relevant cases we have $E \ll k_z^2$, and therefore we can expand

$$\hbar\omega = \frac{\hbar c}{n}\sqrt{k_z^2 + E} \approx \frac{\hbar c}{n}\left(k_z + \frac{E}{2k_z}\right) \equiv E_c + \frac{\hbar^2}{2m_{ph}}E, \tag{11}$$

where the photon mass was defined by (recall that $\frac{c}{n}\hbar k_z \equiv E_c$)

$$\frac{\hbar^2}{2m_{ph}} \equiv \frac{\hbar^2 c^2}{2n^2 E_c}. \tag{12}$$

Thus, the photons become massive particles in respect to the in-plane motion. Within the scalar wave description approximation, and zero boundary conditions on the boundary of the xy-domain, the photons and the excitons obey same equation and, thus, have similar eigenmodes and spectrum, - up to the different effective mass. Therefore, photon-exciton coupling is diagonal in the eigenmode index, while a flat exciton dispersion can be used because of the relatively large mass of the latter.

C. Experimental values of the physical parameter used in the calculations

Explain here how the physical values were deduced from the measurements...

From MATLAB routine:

$w_a = 3.5\,\mu$m Transverse width of the A-letter
$w_b = 2.04\,\mu$m Transverse width of the A-letter
LL=1.35; % Letter length(mkm)
smth_scale=2*1.07/8; %0.22*1.07/8; %1.3*1.07/8; % Smoothness scale in inits of the letter length (1.07/8 - to match the experiment)
% Define recoil energy for photons (not polaritones):
Ex=1581.7+1*0.4; % Exciton energy E_x [in meV]
Ec=1575.7-0.5*1; % Photon 1st band energy (modified from usual "ground" energy!) E_c [in meV]
n_ref=3.25-0.; %3.15; % Effective refraction index
% Photon recoil energy [meV]:
E_r_ph=0.5*(1.054*10^(-34))^2*(3*10^8/n_ref)^2*(pi/2/LL*10^6)^2/Ec/(1.6*10^(-19))^2*10^6;
% link between the Rabi frequency and the Ec energy
E_b1=1570.8; % Energy of the 1st polariton band (in the experiment) [meV]
E0=Ex-E_b1; % Difference between the excitonic level and the 1st polaritonic band
detuning_0=Ec-Ex; % Detuning at k=0
% Calculate Rabi frequency (exciton-photon coupling), which is not independent of
% Ex and Ec, once E_b1 is fixed:
Omega=-detuning_0*sqrt((1+2*E0/detuning_0)^2-1) % Rabi frequency [meV]

III. MAPPING THE 2D WAVE GUIDE PROBLEM TO AN EFFECTIVE 1D PROBLEM

A. Exact 2D formulation

As discussed above, to a very good approximation, both excitons and photons live in a 2D xy-domain. The latter is a symmetric strip with the longitudinal coordinate $x \in [0, L]$, where L is the wire length, and the transverse coordinate $-\frac{w(x)}{2} \leq y \leq \frac{w(x)}{2}$, where the function $w(x) > 0$ defines the x-dependent width of the wire. For constant $w(x)$ the problem is separable and one obtains uncoupled transverse modes. We a interested in $w(x)$ described by a quasiperiodic sequence of the segments of two types, A and B, as already discussed above. To keep the treatment as simple as possible, and also to be able to refer to the known results for the 1D quasi-periodic systems [**Refs**], we wish to map approximately the 2D problem (9) on the strip to a 1D problem with an effective 1D potential $V(x)$. This task is well defined for the low energy states of a sufficiently narrow strip, i.e. when the lowest transverse mode is weakly coupled to the higher ones.

To this end, the exact solution is written in the general form of the Fourier series over the transverse quasi-modes

$$\psi(x,y) = \sum_{n=0}^{\infty} \psi_n(x) \sqrt{\frac{2}{w(x)}} \cos\left[k_{y,n}(x)\, y\right], \quad k_{y,n}(x) = \pi \frac{2n+1}{w(x)}. \tag{13}$$

Here the wave vector $k_{y,n}(x)$ and the expansion coefficients $\psi_n(x)$ depends on x. This is a symmetric solution relative to the middle line $y = 0$, which is uncoupled form the similar anti-symmetric one [for a general-shape strip, both modes would participate in the expansion (13)]. We need the former, since we want to consider the lowest frequency branch, corresponding to the symmetric mode with the smallest wave vector component $k_{y,0}(x) = \frac{\pi}{\max_x w(x)}$. Standartly, (13) is substituted into (9), multiplied by $\sqrt{\frac{2}{w(x)}} \cos\left[k_{y,m}(x)\, y\right]$ and integrated over y. This yields an infinite hierarchy of the coupled ordinary differential equations for $\psi_m(x), \quad m = 0, 1, 2, \ldots$ [the trivial but tedious integration is done in Mathematica]:

$$\begin{aligned} E\psi_m(x) = &\left[-\frac{d^2}{dx^2} + \frac{\pi^2(1+2m)^2}{w^2(x)} + \frac{3+\pi^2(1+2m)^2}{12}\left(\frac{w'(x)}{w(x)}\right)^2\right]\psi_m(x) + \\ &+ \sum_{\substack{n=0 \\ n\neq m}}^{\infty} \frac{(-1)^{n+m}(1+2n)(1+2m)}{2(n-m)(1+n+m)} \left[\left(\frac{w''(x)}{w(x)} + 2\frac{w'(x)}{w(x)}\frac{d}{dx}\right) + \frac{1+n+n^2+3m+3m^2}{(n-m)(1+n+m)}\left(\frac{w'(x)}{w(x)}\right)^2\right]\psi_n(x), \end{aligned} \tag{14}$$

which can also be rewritten in a more symmetric and explicitly Hermitian form as

$$E\psi_m(x) = \left[-\frac{d^2}{dx^2} + \frac{\pi^2(1+2m)^2}{w^2(x)} + \frac{3+\pi^2(1+2m)^2}{12}\left(\frac{w'(x)}{w(x)}\right)^2\right]\psi_m(x) + \\ + \sum_{\substack{n=0 \\ n\neq m}}^{\infty} \frac{(-1)^{n+m}(1+2n)(1+2m)}{2(n-m)(1+n+m)}\left[\left(\frac{d}{dx}\frac{w'(x)}{w(x)} + \frac{w'(x)}{w(x)}\frac{d}{dx}\right) + \frac{1+2\left(n+n^2+m+m^2\right)}{(n-m)(1+n+m)}\left(\frac{w'(x)}{w(x)}\right)^2\right]\psi_n(x), \tag{15}$$

which has symmetric and antisymmetric components, which both can be seen to yield a symmetric matrix element of the Hamiltonian (the anti-symmetric part has $\frac{d}{dx}$, therefore the entire expression is Hermitian).

B. Single lowest transverse mode approximation for low energies

Keeping only the lowest mode $m = 0$, and discarding in it all the terms with $n > 0$, one obtains for $\psi_0(x)$

$$E\psi_0(x) = \hat{H}_{00}\psi_0(x) = \left[-\frac{d^2}{dx^2} + \frac{\pi^2}{w^2(x)} + \frac{\pi^2+3}{12}\left(\frac{w'(x)}{w(x)}\right)^2\right]\psi_0(x), \tag{16}$$

which defines the effective 1D potential along the strip for the lowest transverse mode (note that $w(x)$ is always finite, so that its logarithmic derivative is finite if $w'(x)$ is finite). The strip shape is depicted schematically in Fig. 1(a) as a sequence of the sharp steps, while the actual etching process evidently introduces some smoothness into the width variation. The smoothness scale was used as a tuning parameter of the calculations.

The first term of the potential in (16) is the usual slow-variation approximation, proportional to $k_{y,0}^2(x)$. In out case such an approximation is not sufficient, as can be anticipated already from the expected relative magnitudes of the two terms in the geometric potential in (16). This point is examined in detail numerically in Section VI E below.

Formally, single-mode approximation (16) is justified for low in-plane energies such that coupling to the next transverse mode can be neglected. The following generalizations below to include the coupling should help to quantify the validity of the single-mode approximation. The relation between the approximation (16) and the (supposedly) exact 2D calculation is also examined numerically in Section VI F below. The bottom line is that the higher modes have to be taken into the account for sharp enough waveguide geometry.

C. Two-mode approximation

The 2nd term in (16) becomes singular for very sharp variations of the waveguide geometry, and the next higher transverse mode(s) should be included into the consideration. This was seen by 2D numerical calculation to regularize (or to "soften") the effect of the 2nd term in the single-mode approximation (16).

Let us take into account the next mode to the lowest one, discarding their coupling to other higher modes. Then, in the two-mode approximation the stationary equation reads

$$E\begin{pmatrix}\psi_0(x)\\ \psi_1(x)\end{pmatrix} = \begin{bmatrix}\hat{H}_{00} & \hat{H}_{01}\\ \hat{H}_{10} & \hat{H}_{11}\end{bmatrix}\begin{pmatrix}\psi_0(x)\\ \psi_1(x)\end{pmatrix}, \tag{17}$$

where the Hamiltonian elements are defined from (15) for $n, m \in \{0, 1\}$. We can express $\psi_1(x)$ in terms of $\psi_0(x)$ using the Green's function of $\hat{H}_{11}$. Namely, for the second line in (17),

$$E\psi_1(x) = \hat{H}_{10}\psi_0(x) + \hat{H}_{11}\psi_1(x), \tag{18}$$

we express $\psi_1(x)$ as

$$\psi_1(x) = \frac{1}{E-\hat{H}_{11}}\hat{H}_{10}\psi_0(x) \equiv \hat{G}_{11}(E)\,\hat{H}_{10}\psi_0(x). \tag{19}$$

The important point is that the Green's function $\hat{G}_{11}(E)$ does not have poles for energies E below the spectrum of $\hat{H}_{11}$, therefore $\hat{G}_{11}(E)$ exists on the real axis and the solution for $\psi_1(x)$ is determined unambiguously by $\psi_0(x)$ as a

sourse term [to clarify, this is because for energies below the spectrum of $\hat{H}_{11}$ there are no solutions (eigenmodes) for the homogeneous equation $\left(E-\hat{H}_{11}\right)\psi_1(x)=0$ which satisfy the boundary conditions (finite on $\pm\infty$ for the infinite system)]. This allows for the reduction of the 2-mode approximation to the effective 1D description given in the next sub-section (actually, the same could by done for any n-mode approximation as well).

D. Solving the transmission problem for 2-mode (n-mode) approximation

In this subsection some aspects of the calculation of the transmission properties are considered, motivated by the experiment with the constriction (the "diod") [5]. The transmission (or scattering) rather than eigenvalue problem should be considered in the experiment such as with the constriction geometry. Assuming the one-side incidence (which is usually of the interest), in the purely 1D case the procedure is to define the outgoing wave boundary condition on the transmission side and find the corresponding solution on the incidence side, which yields the transmission coefficients for any energy. In the quasi-1D case with n-channel (same as n-mode) leads the transmission solution lives in the n-dimentional space if all n channels are open. Numerically, the corresponding basis can be found by solving for n linearly independent outgoing boundary conditions with a non-zero amplitude each time in one of the channels. On the other hand, if only one channel is open for the free propagation at a given considered energy, then the transmission solution is one-dimensional, since the remaining (closed) channels give only the evanescent contributions (decaying exponents) related unambiguously to the open channel solution (assuming no bound states, see (19) above). The question is: does one still need to solve numerically for n independent outgoing (or decaying) wave boundary conditions, or there is a way to do it only once (probably approximately - see below)?

Simple situation as it is, it puzzles me a bit. The possible alternatives are as follows:

1. The straightforward approach is to solve for independent n outgoing boundary conditions. For the closed channels, the general solution in the lead as a combination of the growing and decaying exponentials, and only the latter should appear in the transmitted wave. Then, solving n times for the outgoing/decaying boundary condition with a single channel populated each time, one obtains n solutions. From the latter a unique linear combination can be constructed in which the exponentially growing terms in the closed channels on the incidence side are eliminated (which would be present in each one of the basic solutions). This combination is the required scattering solution, from which the transmission amplitude for the open channel can be determined. This the "theoretical" recipe for the numerical solution. In practice it may proof impractical because of the very pour numerical stability. Namely, in contrast to the positive energy case, now the closed channels are solved for the negative (here: below the "self"-spectrum) energies, for which the basic homogeneous solutions are the growing and the decaying exponents. If the growth rate of the latter is large (e.g., for the large negative energy), then the numerical errors would grow fast as well, which could be a problem for a long enough system (seemingly not a problem for the case of the constriction [5]). Namely, by the procedure described above the divergent tails in the leads would be eliminated, but the solution in the scattering region and, thus, the transmission coefficient of the open channel will be wrong. This problem seems to be solved in the Green's function approach using (19) [see item (3) below].

2. Intuitively it seems strange that described in item (1) solution for n boundary conditions is required, while only one *physically* meaningful solution exists (however, still there are $n-1$ additional non-physical, i.e. diverging at ∞ solutions). Initially I thought that, because physically the evanescent channels are "populated" only owing to the existence of the propagating lowest mode as source, Eq. (19), it is enough to solve for the boundary condition of the outgoing wave in the open channel only and zero in the closed channels. This approximation neglects the exponentially decaying terms in the closed channels, the effect of which could be naively thought small (?). But then I realized that such a solution would have a divergent to ∞ contribution on the side of the insidence, which should be eliminated by subtracting some other linearly independent solution. The latter would generally change the solution in the scattering region and the transmission coefficients. Thus, such an approximation is in general not good.

   In general, probably there is no such a straightforward shortcut, as could be seen from the simple 1D case with, e.g., zero potential and a source term at a finite support. The genaral solution is a sum of some particular nonhomegeneous solution and a general linear combination of the two independent homogeneous ones:

$$f_{\text{general}}(x)=f_{\text{part,nonh}}+Af_{1,\text{hom}}+Bf_{2,\text{hom}}. \tag{20}$$

   For $E<0$, the particular nonhomegeneous solution satisfying the boundary conditions is unique, while both homogeneous ones diverge at $\pm\infty$. We need the former one, which is physical. Numerically, one have to solve

twice: the homogeneous and the nonhomogeneous equations with some (e.g. same) decaying BC at one side of the source and, then, construct a linear combination of them to eliminate the diverging exponent on the other side of the source. So, seemingly there is no simple shortcut.

3. Finally, the problem can be made effectively 1D while taking into the account the higher modes, as described in detail in the next subsection. This is done, e.g. for $n = 2$, by plugging the solution (19) into (17). The effective 1D potential is now non-local and depends on the Green's function which should be found or approximated (using some approximation seems to be practical, - see next subsection). If the later is done, however, the purely 1D approach to the scattering can be applied. There is no problem of the divergent terms in the solution (19), since the Green's function is constructed only of the eigenstates satisfying the boundary conditions.

IV. NEXT MODE CORRECTION TO THE 1D SINGLE-LOWEST-MODE APPROXIMATION

A. Formally exact reduction of the quasi-1D 2-mode problem to the 1D single-mode problem

As said above, second transverse mode is required to regularize (or to "soften") the effect of the 2nd term in the single-mode approximation (16) when the waveguide width geometry becomes rather sharp, - even when considering the lower part of the spectrum. The question now is how to take into the account the effect of the next transverse mode and still to remain in the effective 1D single-mode approximation.

As explained in the preceeding subsection, for the energies below the spectrum of $\hat{H}_{11}$, the physical solution for $\psi_1(x)$ is related unambigously to $\psi_0(x)$ by (19). Therefore, for such energies (below the spectrum of $\hat{H}_{11}$), we can substitute (19) into the first line in (17) to obtain the (effective) 1D problem equation for $\psi_0(x)$ only:

$$E\psi_0 = \left[\hat{H}_{00} + \hat{H}_{01}\hat{G}_{11}(E)\,\hat{H}_{10}\right]\psi_0, \tag{21}$$

which is written deliberately in the operator notation, since the operator $\hat{H}_{01}\hat{G}_{11}(E)\,\hat{H}_{10}$ is not local anymore in the position representation (i.e., the equation for $\psi_0(x)$ in the position representation involves now an integral).

Equation (21) can be considered in a two-fold way (from the two points of view):

- as a scattering problem for an infinite system, when E is a fixed parameter (see previous subsection). In this case the energy is fixed, and we can use some approximation for the Green's function with an actual value of E (or, to calculate numerically the Green's function for the given E).
- as an eigenvalue problem for finite system with a given BC. In this case, it is now a non-linear eigenvalue equation, where one can try different simplifying approximations for $\hat{G}_{11}(E)$ to get rid of the non-linearity in E (for example: replacing E by some constant value E_0, e.g. a ground energy of the lowest transverse mode, and/or replacing $\hat{G}_{11}(E)$ by $E_0^{-1}\delta(x_1 - x_2)$ with some E_0 etc., - see below).

The effecive 1D equation (21) is valid for the energies below the spectrum of $\hat{H}_{11}$ so that the second mode channel is closed. The bottom of the spectrum of $\hat{H}_{11}$ lies for sure above the value minimal value of the "geometrical" potential in $\hat{H}_{11}$, i.e. above $\min k_{y,1}^2(x) = \left(\frac{3\pi}{\max_x w(x)}\right)^2$, so that the above reduction is applicable at least for

$$E < \min k_{y,1}^2(x) = \frac{9\pi^2}{\max w^2(x)}, \tag{22}$$

where the energy is counted from E_c of the vertical (z) confinement.

B. Delta-function approximation for the Green's function

For the energy E well below the spectrum of $\hat{H}_{11}$ (see Appendix D)

$$G_{11}(x_1, x_2, E) \approx \frac{1}{E - E_0^{(11)}}\delta(x_1 - x_2), \tag{23}$$

where, for certainty, the energy refference point $E_0^{(11)}$ is the bottom of the spectrum of H_{11} (conf. D10). Plugging this approximation into (21) gives a local equation for $\psi_0(x)$

$$E\psi_0(x) = \left[H_{00}(x) + \frac{1}{E - E_0^{(11)}} H_{01}(x) H_{10}(x)\right] \psi_0(x). \tag{24}$$

For a given fixed energy this can be solved to obtain a scattering solution, and the second term in (24) is just a correction to the effective potential. On the other hand, (24) is still a non-linear eigenvalue problem, where the "parametric" approximation can be used. The latter amounts to replacing the energy on the right hand side by some fixed value, so that the result is expected to be valid in vicinity of this value. For example, $E - E_0^{(11)}$ on the r.h.s. of (24) could be replaced with the energy difference between the bottoms of the spectra of H_{00} and H_{11}, e.g. estimated as

$$E_0 \equiv E_0^{(11)} - E_0^{(00)} = \left(\min k_{y,1}^2(x) - \min k_{y,0}^2(x)\right) = \frac{8\pi^2}{\max w^2(x)}, \tag{25}$$

i.e. the difference between the minima of the geometric potentials in H_{00} and H_{11}. Then, in the *local* and *parametric* approximation for $G_{11}(x_1, x_2, E)$, one obtains in the x-representation

$$E\psi_0(x) = \left[H_{00}(x) - \frac{1}{E_0} H_{01}(x) H_{10}(x)\right] \psi_0(x). \tag{26}$$

Although it does not prove to be a good approximation (becasue of the locality - see below), let us write down explicitly the above equation. From Eq. (14), the operators $\hat{H}_{01}(x)$ $[m = 0, n = 1]$ and $\hat{H}_{10}(x)$ are, [note that $\left(\hat{H}_{01}\right)^\dagger = \hat{H}_{10}(x)$]:

$$\hat{H}_{01}(x) = -\frac{3}{4}\left[\frac{3}{2}\left(\frac{w'(x)}{w(x)}\right)^2 + \frac{w''(x)}{w(x)} + 2\frac{w'(x)}{w(x)}\frac{d}{dx}\right] \tag{27}$$

$$= -\frac{3}{4}\left[\frac{7}{2}\left(\frac{w'(x)}{w(x)}\right)^2 - \frac{w''(x)}{w(x)} + 2\frac{d}{dx}\frac{w'(x)}{w(x)}\right], \tag{28}$$

$$\hat{H}_{10}(x) = -\frac{3}{4}\left[\frac{7}{2}\left(\frac{w'(x)}{w(x)}\right)^2 - \frac{w''(x)}{w(x)} - 2\frac{w'(x)}{w(x)}\frac{d}{dx}\right], \tag{29}$$

using which one obtains (see Appendix B)

$$\hat{H}_{01}(x)\hat{H}_{10}(x) = \frac{9}{16}\left\{-\frac{35}{4}\left(\frac{w'(x)}{w(x)}\right)^4 + 18\frac{w''(x)}{w(x)}\left(\frac{w'(x)}{w(x)}\right)^2 - \left(\frac{w''(x)}{w(x)}\right)^2 - 2\frac{w'(x)}{w(x)}\frac{w'''(x)}{w(x)} - 4\frac{d}{dx}\left(\frac{w'(x)}{w(x)}\right)^2\frac{d}{dx}\right\}, \tag{30}$$

The above expression gives the correction to the single-mode equation (16) for ψ_0 due to its coupling to the next transverse mode ψ_1, Eq. (26), in the local (23) and the parametric (26) approximations for the Green's function $G_{11}(x_1, x_2, E)$. Finally, inserting the obtained terms into the wave equation (26) yields

$$E\psi_0(x) = \left[-\frac{d}{dx}\left\{1 - \frac{9}{4E_0}\left(\frac{w'(x)}{w(x)}\right)^2\right\}\frac{d}{dx} + \frac{\pi^2}{w^2(x)} + \frac{\pi^2+3}{12}\left(\frac{w'(x)}{w(x)}\right)^2 + \right.$$
$$\left. + \frac{9}{16E_0}\left\{\frac{35}{4}\left(\frac{w'(x)}{w(x)}\right)^4 - 18\frac{w''(x)}{w(x)}\left(\frac{w'(x)}{w(x)}\right)^2 + \left(\frac{w''(x)}{w(x)}\right)^2 + 2\frac{w'(x)}{w(x)}\frac{w'''(x)}{w(x)}\right\}\right]\psi_0(x). \tag{31}$$

1. *A note: position-dependent mass*

Apart of the generally fourth order of the derivative of the width, this "coupling" correction contains also the differential operator. The latter introduces the position dependent mass (here dimensionless) into the Schrodinger-like equation (**??**) for ψ_0, i.e.

$$-\frac{d^2}{dx^2} \to -\frac{d}{dx}\left[1 - \frac{9}{4E_0}\left(\frac{w'(x)}{w(x)}\right)^2\right]\frac{d}{dx} \equiv -\frac{d}{dx}\frac{1}{M(x)}\frac{d}{dx}. \tag{32}$$

Here, the position dependent inverse mass may, generally, go to zero and become negative. Some artificial examples of such cases can be examined analytically, e.g. for the piece-wise-constant mass (and zero potential), where one needs to match obvious solutions for the intervals with constant mass (the condition is on the wave function continuity and jump in its first derivative). Numerical tests in Mathematica gave reasonable solutions for the step-wise sign-changing mass, but have encountered a problem when the inverse mass goes smoothly from positive to negative. The latter is, probably, due to the numerical integration scheme not adapted to the case of the vanishing coefficient of the derivative operator (this should be kept in mind shall the above equation be solved numerically as a Cauchy problem). The possibility of the vanishing and negative mass seems, however, be irrelevant to the present context. This is because, as discussed below, it turns out that in order to improve the approximation either the pre-factor E_0^{-1} of the mode-coupling correction terms should be greatly decreased, or the locality approximation for the Green's function given up. As a result, the second term in the inverse mass in (32) decreases greatly.

The equation form in (31), i.e. with a position dependent mass, is convenient for the numerical diagonalization (namely, it is convenient for the calculation of the matrix elements of the Hamiltonian). However, using the transformation

$$\psi_0(x) = f(x)\,\phi(x), \tag{33}$$

it is easy to obtain an equation for $\phi(x)$ with the position-dependent coefficient in front of the second derivative with no first derivative present. The required function is (see Appendix C)

$$f = \frac{1}{\sqrt{1 - \frac{9}{4E_0}\left(\frac{w'(x)}{w(x)}\right)^2}}. \tag{34}$$

The resulting equation for $\phi(x)$ is given in Appendix C. It not clear, however, whether this form is useful (in particular, because it now contains potential divergent at the points where f diverges).

C. Empirical regularization-correction to the Delta-function approximation

The described above δ-function approximation for the Green's function turned out completely unacceptable when applied as is to calculate the spectrum of, e.g. the Fibonacci waveguide with a reasonable degree of smoothness of the geometry (using also the parametric approximation for E, which by itself is appropriate). The details are given below in the numerical section. In short, it resulted in a huge negative shift of the spectral edge and the band structure ridiculously stretched to that scale. This is a consequence of the exaggerated and mostly negative-signed coupling correction to the potential [both locally and on-the-average; the inverse mass also became negative somewhere, but this did not help the final result]. Below, are mentioned the phenomenolgical corrections applied to patch the deficiency of the approximation.

Numerical observations:

- The failure of the δ-function approximation can be cured surprisingly well by tuning (decreasing) the magnitude of the coupling correction term (30). This was done by increasing the magnitude of E_0 in the denominator of (31). The required "regularization" factor depends on the smoothness of the waveguide geometry (which is each time uniform in the considered set-up) and is very large, e.g., $E_0 \sim 60E_r$ and $E_0 \sim 540E_r$ for the smoothenss scales $\{1, 0.25\} \times 1.07/8a$ respectively instead of the initially taken $E_0 \sim 4.5E_r$ (mode separation is about $5E_r$). This regularization is very sensitive to the specific chosen value of E_0. On the other hand, this correction could be parametrized phenomenologically as

$$E_0 \Rightarrow \left(\frac{0.6}{S_m \times 1.07/8}\right)\left(11 + 19\left(\frac{0.25}{S_m}\right)^2\right) E_r, \tag{35}$$

  where E_r is the recoil energy and S_m the smoothness parameter. Here the first factor is attributed to the smoothing action of the Green's function on the term in the potential, and the second one is attributed to the normalization of the Green's function. Thus, using such a regularization would be impractical in the geometry with a non-uniform smootheness scale of the width variation. Moreover, any reasonable explanation of it appeals to the smoothing effect of the non-local Green's function. Although so calculated E_0 is relatively close to the height of the peak of the geometric potential in H_{11} ($\sim 42E_r$ and $\sim 500E_r$ for the quantitative examples for E_0 given above before Eq. (35)), the corresponding δ-function approximation does not fit at all into the numerically calculated Green's function (in regard to an order of magnitude smaller normalization integral).

- The δ-function approximation can be abandoned in favour of the non-local Green's function in the free particle approximation (see Appendix D). The normalization and the spatial decay scale of the latter was adjusted empirically to the numerically calculated exact Green's function $\hat{G}_{11}(E)$. The adjustment of the normalization should be done separately for each smoothness scale. The result for the energy spectrum was good, but very sensitive to the normalization value. Thus, this approach is, again, both empirical and not practical.

- In the non-local approximation for the Green's function, the non-locality may be applied either fully, i.e. also to the wavefunction, or partially, i.e. only to the terms in the correction $\hat{H}_{01}\hat{G}_{11}(E)\hat{H}_{10}$. The latter is justified assuming slow variation of the wavefunction (in this case the notion of the effective local potential is still applicable). In all the numerical tests the difference between the two calculcations was rather negligible, - inspite of the fact that higher energy states vary on the scale compared to the smoothness scale (but the difference became more noticable in the new system Wire_18 with smaller letter length).

- Finally, instead of the described above hand-waving approximations for the Green's function, the analytical expression for the later was derived used a simplified model for the geometrical potential barrier. This approximation, described in detail in the next subsection, is controlable, requires a minimal adjustment, and gives acceptable results for the energy spectrum.

- Equivalence of the final result of the methods described above (either justifiable or not) suggests that in the considered numerically cases the precise form of, let's say, effective potential is not very important (more precisely, it so for low energies). It seems that, especially in view of the low energies at the focus, the important thing is a presence of the narrow disturbance in the effective potential at the position of the fast change in the waveguide width. The precise form of the disturbance does not matter, but its effective strength (e.g. its integral) should be estimated correctly. This is my explanation to why quite different approximations but with different parameters give very similar results.

D. Non-local approximations for the Green's function $\hat{G}_{11}(E)$

1. *Does the Green's function in $\hat{H}_{01}\hat{G}_{11}(E)\hat{H}_{10}$ produce the smoothing effect*

Initially I thought erroneously that non-locality of the Green's function in the combination $\hat{H}_{01}\hat{G}_{11}(E)\hat{H}_{10}$ means necessarily an effect of smoothing (by the convolution) of the fast varying terms in both $\hat{H}_{01}$ and $\hat{H}_{10}$. That this is not so can be seen from the next simple example. Let $H_{01}(x) = u\delta(x - x_0)$ and $H_{10}(x) = \sum_{n=1}^{N} v_n \delta(x - x_n)$ be local, and consider

$$\left\langle x \left| \hat{H}_{01}\hat{G}_{11}(E)\hat{H}_{10} \right| \psi \right\rangle = \int dx'' u\delta(x - x_0) G(E, x, x'') \sum_{n=1}^{N} v_n \delta(x'' - x_n)\psi(x'')$$
$$= u\delta(x - x_0) \sum_{n=1}^{N} v_n G(E, x, x_n)\psi(x_n). \tag{36}$$

First, even if $N = 1$ and $x_1 = x_0$, then $\left\langle x \left| \hat{H}_{01}\hat{G}_{11}(E)\hat{H}_{10} \right| \psi \right\rangle = uv_1\delta(x - x_0)G(E, x_0, x_0)\psi(x_0) = uv_1\delta(x - x_0)G(E, x_0, x_0)\psi(x)$ may not be interpreted as an action of the altogether smoothed potential, since it is proportional to $\delta(x - x_0)$ [although it is indeed more regular than $\delta^2(x - x_0)$]. Second, it is also not correct to think that $\hat{G}_{11}(E)$ acts to smooth the terms in $\hat{H}_{10}$. E.g., for the same special case $N = 1$,

$$\left\langle x \left| \hat{G}_{11}(E)\hat{H}_{10} \right| \psi \right\rangle = G(E, x, x_0)\psi(x_0) \neq G(E, x, x_0)\psi(x), \tag{37}$$

i.e., it is not the function $\psi(x)$ multiplied with a smooth function $G(E, x, x_0)$. In the same way, $\sum_{n=1}^{N} v_n G(E, x, x_n)\psi(x_n)$ in Eq. (36) has nothing to do with the smoothed function $H_{10}(x) = \sum_n v_n \delta(x - x_n)$ if $\psi(x_n)$ varies fast on the scale of the width of $G(E, x_1, x_2)$. Saying simply, action of $\hat{G}_{11}(E)$ smoothes the product $H_{10}(x)\psi(x)$, but not $H_{10}(x)$ separately.

The simplification comes if $\psi(x)$ may be assumed to vary slowly of the scale of the width of $G(E, x_1, x_2)$. This assumption is mostly justified in our case. This is because the geometric potential in H_{11} is very large, so that in the

region of the waveguide width variation (which is only of the importance) $G(E,x_1,x_2)$ decays much faster than the wavelength of the eigenstates of the lowest tansverse mode. Then, writing $H_{01}(x)=V_{01}(x)$ and $H_{10}(x)=V_{10}(x)$

$$\left\langle x\left|\hat{H}_{01}\hat{G}_{11}(E)\hat{H}_{10}\right|\psi\right\rangle = V_{01}(x)\int dx''G(E,x,x'')V_{10}(x'')\psi(x'') \tag{38}$$

$$\approx V_{01}(x)\psi(x)\int dx''G(E,x,x'')V_{10}(x'')\equiv V_{01}(x)\tilde{V}_{10}(x)\psi(x), \tag{39}$$

where $\tilde{V}_{10}(x)=\int dx''G(E,x,x'')V_{10}(x'')$ is indeed the convolution smoothed potential $V_{10}(x)$. Thus, if $\psi(x)$ varies slowly compared to $G(E,x_1,x_2)$, then action of $\hat{H}_{01}\hat{G}_{11}(E)\hat{H}_{10}$ is equivalent to the local potential $V_{01}(x)\tilde{V}_{10}(x)$.

Finally, our operators $\hat{H}_{01}$ and $\hat{H}_{10}$ contain also the differentiation, Eq. (28,29). This, however, does not pose any additional problem. Assuming again that both $\psi(x)$ and $\psi'(x)$ vary slowly compared to $G(E,x_1,x_2)$, one has

$$\left\langle x\left|\hat{G}_{11}(E)\hat{H}_{10}\right|\psi\right\rangle = -\frac{3}{4}\int dx_1G(E,x,x_1)\left[\frac{7}{2}\left(\frac{w'(x_1)}{w(x_1)}\right)^2-\frac{w''(x_1)}{w(x_1)}-2\frac{w'(x_1)}{w(x_1)}\frac{d}{dx_1}\right]\psi(x_1)$$

$$= -\frac{3}{4}\int dx_1G(E,x,x_1)\left[\left(\frac{7}{2}\left(\frac{w'(x_1)}{w(x_1)}\right)^2-\frac{w''(x_1)}{w(x_1)}\right)\psi(x_1)-2\frac{w'(x_1)}{w(x_1)}\psi'(x_1)\right] \tag{40}$$

$$\approx -\frac{3}{4}\int dx_1G(E,x,x_1)\left[\left(\frac{7}{2}\left(\frac{w'(x_1)}{w(x_1)}\right)^2-\frac{w''(x_1)}{w(x_1)}\right)\psi(x)-2\frac{w'(x_1)}{w(x_1)}\psi'(x)\right] \tag{41}$$

$$= -\frac{3}{4}\left\{\int dx_1G(E,x,x_1)\left[\frac{7}{2}\left(\frac{w'(x_1)}{w(x_1)}\right)^2-\frac{w''(x_1)}{w(x_1)}-2\frac{w'(x_1)}{w(x_1)}\frac{d}{dx}\right]\right\}\psi(x), \tag{42}$$

where the convolution smoothing acts only on the functions of x_1, while derivative $\frac{d}{dx_1}$ was replaced by $\frac{d}{dx}$ and thus became local. The derivative inside $\hat{H}_{01}$ in $\hat{H}_{01}\hat{G}_{11}(E)\hat{H}_{10}$ does acts on everything in front of it, but it is local (while in calculation of marix elements $\left\langle m|\hat{H}_{01}\hat{G}_{11}(E)\hat{H}_{10}|n\right\rangle$, cf. Eq. (61), $\hat{H}_{01}$ is applied to the left).

To summarize, in general it is incorrect to think that Green's function smoothes the potential in $\hat{H}_{10}$, but this becomes correct if the operator $\hat{G}_{11}(E)\hat{H}_{10}$ acts on the state which varies in space slow compared to the width of the Green's function. In the latter case, $\hat{G}_{11}(E)\hat{H}_{10}$ can be approximated by a local operator.

2. Constructing the non-local Green's function

Green's function $G(E,x_1,x_2)$ for a 1D Shrodinger equation with some boundary conditions can be constructed from two independent solutions $y_1(x)$ and $y_2(x)$. The latter should satisfy the initial conditions on the left and the right boundaries respectively, which are consistent with the boundary conditions for the Green's function (e.g. for zero BC, $y_1(x=0)=0$ and $y_2(x=L)=0$). The identity relating Green's function to the independent solutions is

$$G(E,x_1,x_2)=\frac{1}{W(E)}\left(y_1(x_1)y_2(x_2)\theta(x_2-x_1)+y_1(x_2)y_2(x_1)\theta(x_1-x_2)\right), \tag{43}$$

$$y_1(0)=0,\quad y_1'(0)=1,\quad y_2(L)=0,\quad y_1'(L)=1,\quad W(E)=y_1(x)y_2'(x)-y_1'(x)y_2(x),$$

where the Wronskian $W(E)$ does not depend on x.

The Green's function is not translation invariant (i.e. it depends on both x_1 and x_2, and not on thier difference x_2-x_1 only). However, we need to determine it primerily in the vicinity of the sharp width changes, i.e. under the corresponding barriers of the geometric potential in H_{11}. This is because H_{01} and H_{10} vanish rapidly outside these regions (and the energy E is assumed low enough so that Green's function is short-range and does not connect neighboring steps). The corresponding potential barriers in H_{11} has some relatively complicated shape determined by the applied smoothing kernel, e.g. (64). The exact $y_1(x)$ and $y_2(x)$ can be calculated numerically, or approximately semi-classically (WKB). Alternatively, in order to have a simple analytical expression, we can use a simplified model of the rectangular potential barrier. By the way, such shape is not completely unrealistic, since it would be obtained for the rectangular smoothing kernel, which could be applied numerically (though analytically it would eventually lead to the appearence of the derivalives of δ-function). An additional slight approximation done is taking equal "shoulders"

of the potential to the left and to the right of the barrier. The above approximations are illustrated in Fig. 11 in the Appendix D 2. Finally, the obtained Green's function is still not translation invariant and not symmetric (with respect to, e.g. fixed x_2) since the barrier has finite width. Therefore, as a last approximation, it is replaced by the symmetric and translation invariant two-sided exponential function, which fits its average peak value and average slope at $x_1 = x_2$ (the average is done over the under-barrier region). The technical details are given in the Appendix D 2. The final result for the effective Green's function is

$$\tilde{G}\left(x_1, x_2, E\right) = -\frac{1}{2k \sinh kx_0}\left[\cosh kx_0 + \frac{\sinh kx_0}{kx_0}\right] e^{-\kappa|x_2 - x_1|}, \tag{44}$$

where the decay exponent is given by

$$\kappa = k\frac{\left(kx_0\right)^2 \sinh kx_0 + kx_0 \cosh kx_0 - \sinh kx_0}{\left(kx_0\right)\left(kx_0 \cosh kx_0 + \sinh kx_0\right)}, k = \left(U - E\right)^{1/2}, \tag{45}$$

with U and x_0 being the barrier height and width (note that in the limit $k \to \infty$, one obtains the free particle result, Eq. (D9), $\tilde{G}\left(x_1, x_2, E\right) = -\frac{1}{2k} e^{-k|x_2 - x_1|}$).

Here U and x_0 characterize the rectagular barrier equivalent to the actual one (see Appendix D 2 for the explanaition). The barrier width and height are parametrized as $x_0 = \beta a$ and $U \sim 1/x_0$ respectively, where a is the letter length and β is proportional to the parameter η in the smoothing kernel (64). Several possible relations between β and η can be devised applying different criterions to matching between the model rectangular and the actual barriers, exemplified in Appendix D 2 [e.g. matching some average value of the potential, or the average value of the complex momentum, etc.]. The optimal relation, however, is (meanwhile) to be obtained from the numerical tests. Numerically, the proper results (for the eigenmode spectrum) were obtained for β given by (D20)

$$\beta = 2^{1/4}\sqrt{\pi}\eta, \tag{46}$$

obtained by matching the mean barrier potentials. The value of the imaginary momentum $k = \left(U - E\right)^{1/2}$ is given in (D39,D40)

$$k = \left[4\left(1 + 2m\right)^2\left(\frac{a}{\bar{w}}\right)^2 + \frac{3 + \pi^2\left(1 + 2m\right)^2}{3\pi^2}\left(\frac{\Delta w}{\bar{w}}\frac{1}{\beta}\right)^2 - 4\left(\frac{a}{w_a}\right)^2\right]^{1/2} E_r^{1/2}, \tag{47}$$

where $\Delta w = w_a - w_b$, $\bar{w} = \frac{w_a + w_b}{2}$ and $E_r = \frac{\pi^2}{4a^2}$ is the recoil energy (for the periodic structure of the period $2a$.

Once the Green's function in (21) is approximated by one having a translationally invariant kernel $\tilde{G}\left(x_1, x_2, E\right)$, it is easy to implement the numerical solution of the eigenvalue problem. The relevant matrix elements are (cf. (58))

$$\left\langle p, q|\hat{H}_{01}\hat{G}_{11}\left(E\right)\hat{H}_{10}|n, m\right\rangle, \tag{48}$$

and the action of the Green's function is realized as a convolution (in the position representation). The convolution may be applied to the function $\left\langle x|\hat{H}_{10}|n, m\right\rangle$, or, approximately, only to some terms in $H_{10}\left(x\right)$ according to Eq. (42).

It could be a little bit more tricky to solve, for example, the Cauchy problem using the non-local, though trnaslationally invariant Green's function. It seems, however, that an approximation like in Eq. (42) could be done to obtain an effective local 1D potential.

The spectrum is calculated by the numerical diagonalization of the effective 1D Hamiltonian matrix evaluated in the basis $\left\{\phi_n\left(x\right) = \sin\frac{\pi n x}{L}\right\}_{n=1}^{N}$. Consider the matrix element of the correction term $\hat{H}_{01}\hat{G}_{11}\left(E\right)\hat{H}_{10}$, using $\hat{H}_{01} = \hat{H}_{01}^{\dagger}$ and the short notation for position representation (29)

$$\hat{H}_{10}\left(x_1, x_2\right) = \delta\left(x_1 - x_2\right)\left[F\left(x\right) + Q\left(x\right)\frac{d}{dx}\right],$$

$$\left\langle \phi_n|\hat{H}_{01}\hat{G}_{11}\left(E\right)\hat{H}_{10}|\phi_m\right\rangle = \left\langle \hat{H}_{10}\phi_n|\hat{G}_{11}\left(E\right)\hat{H}_{10}|\phi_m\right\rangle = -\frac{1}{E_0}\int dx' dx'' \Phi_n^*\left(x'\right) g\left(x' - x''\right) \Phi_m\left(x''\right),$$

with

$$\Phi_n\left(x\right) \equiv \left[F\left(x\right) + Q\left(x\right)\frac{d}{dx}\right]\phi_n\left(x\right). \tag{49}$$

Let us assume that $g\left(x'-x''\right)$ is a Gaussian-like function and can be represented as an auto-convolution,

$$g\left(x'-x''\right)=\int dxg\left(\sqrt{2}\left(x'-x\right)\right)g\left(\sqrt{2}\left(x-x''\right)\right), \tag{50}$$

of similar functions, but narrower by the factor $\sqrt{2}$. Then the matrix element can be written as

$$\left\langle \phi_n|\hat{H}_{01}\hat{G}_{11}\left(E\right)\hat{H}_{10}|\phi_m\right\rangle =-\frac{1}{E_0}\int dx\tilde{\Phi}_n^*\left(x\right)\tilde{\Phi}_m\left(x\right), \tag{51}$$

where tilde means the convolution (smoothing)

$$\tilde{\Phi}_n\left(x\right)\equiv\int dx'g\left(\sqrt{2}\left(x-x'\right)\right)\Phi_n\left(x''\right).$$

E. Numerical calculations

Numerical calculation was tested on the Fibonacci system S_{11} and it has been developed in several iterations (here it is given in the "historical" perspective):

1. First, the δ-function approximation (23,31) for the Green's function was applied. This resulted in over-estimation of the the effect of the correction. Namely, the lower spectral edge has shifted strongly downwards and fragmentation of the band structure has decreased. The value of the energy parameter E_0 was taken according Eq. (25).

2. To correct the overshooting described in the previous item, the energy parameter E_0 was defined as the difference in the mean geometric potentials in H_{11} and H_{00} (which was quite larger than due to Eq. (25)), and the correction term was additionally decreased (moderated) by multiplying it by the factor

$$\left(\frac{\sqrt{2}\alpha}{d_G}\right)^2, d_G=0.68 \tag{52}$$

   where α is the waveguide geometry smoothness scale in units of the letter length. The parameter $d_G=0.68$ was thought as the typical width of the actual Green's function (it was adjusted experimentally, but had a reasonable value). This moderation seemed to do the job in relatively broad range of the smoothness scales $\alpha=\{0.5,1,2\}\times(1.07/8)$. The (wrong) logic was to think the Green's function as a Gaussian represented as a convolution of two Gaussians narrower by the factor $\sqrt{2}$. Then, each one of the two will act by smoothing H_{01} and H_{10} respectively and thus reducing the their narrow peaks by about the factor $\sqrt{2}\alpha/d_G$. The square of this gives the applied correction coefficient. Logically, this was wrong already because the factor was applied to the matrix element implying an integration, because of which the widening of the peak also introduces an additional factor $\sim d_G/\alpha$. Therefore, squaring the the factor (α/d_G) was not justified, while without it the correction did not work (actually, the efficiency of the applied coefficient is, probably, related to the presence of the term w'' in the smoothed function).

3. The absence of the explanation of the correction described in the previous item enforced using a non-local approximation of the Green's function. An approximation of the free (and non-local) Green's function was used (see Appendix D),

$$G_0\left(E=-\kappa^2<0,x_1,x_2\right)=-\frac{1}{E}\frac{\kappa}{2}e^{-\kappa|x_1-x_2|}, \tag{53}$$

   but with an additional numerical normalization factor deduced from the numerical calculation of the actual Green's function for H_{11}. Namely, the integral of G_0 over x_1 is exactly $-E^{-1}$, while integral of the actual Green's function depends on x_2 and is smaller by the factor which depends both on E and the smoothness of the waveguide geometry (because the latter affects geometric potential in H_{11}).

V. THE EFFECTIVE 1D GEOMETRIC POTENTIALS

It is usefull to give here and to compare numerically the three levels of the approximations for the effective 1D potential for the lowest transverse mode: the adiabatic approximation, the single mode appoximation (16) and the one corrected due to the coupling to the second transverse mode.

.....

The initial calculations started from essentially the adiabatic approximation with the parameters provided by the experimentalists (remove this or put into the Appendix):

We use here the configuration tabbed in the presentation as "Family 1", i.e. with wider/narrower strip at letters A/B, corresponding to

$$V_A = 0, \text{ and } V_B = V_0. \tag{54}$$

We take the following values, corresponding to Fib2:

$$a = 1.35\,\mu\text{m}, \quad V_0 = 1\,\text{meV}\,. \tag{55}$$

The recoil energy (**??**) is estimated using the polariton mass quoted from [1]

$$M = 4.5 \times 10^{-5} m_0 \quad \rightarrow \quad E_R = 1.15\,\text{meV}\,. \tag{56}$$

This yields the dimensionless height of the potential step $\tilde{V}_0 = V_0/E_R = \frac{1}{1.15}$. As demonstrated below, seemingly better agreement between the numerical calculations and the experimental data is obtained for larger value of $\tilde{V}_0$ by factor of about $1.5 \div 2$. Probably, we should use the correspondingly bigger value of the polariton mass (see also Appendix B). To cover this uncertainty, below we give numerical results for three different values of $\tilde{V}_0$:

$$\tilde{V}_0 = \frac{V_0}{E_R} = \frac{1}{1.15}, \frac{1.5}{1.15}, \frac{2}{1.15}. \tag{57}$$

For the same reason, in most cases below we give the results in the energy scale in units of E_R, and not in meV (evidently, this can be interpreted as either modifying V_0 or E_R).

VI. FULL 2D CALCULATION

This section describes the full 2D calculation of the eigenenergies and the eigenfunctions. First, the technical details are given such as the basic expressions and the convergence of the calculation. Then, considering the 2D calculation as exact, the physical aspects are discussed such as the importance of the transverse mode coupling for the spectrum and the eigenmodes, and the effect of the smoothness of the waveguide geometry on the eigenspectrum. Finally, the 2D calculation is used as a reference for the different 1D approximation schemes.

A. Basic expressions

The basic equation is already given above in Eq. (15). The numerical calculation, however, is done be the direct diagonalization of the truncated Hamiltonian matrix evaluated in the (generalized) Fourier basis (cf. Eq. (13))

$$\phi_{mn}(x,y) = \sum_{n=0}^{N_n} \sum_{m=1}^{N_m} \sqrt{\frac{2}{w(x)}} \sin\frac{\pi m x}{L} \cos\frac{\pi(2n+1)\,y}{w(x)}, \tag{58}$$

where L is the waveguide length and zero boundary conditions at $x = 0, L$ are assumed. The y-dependence has been discussed above. Parameters N_n and N_m define the truncation of the basis (see the next subsection). Then, the eigenmodes are given by

$$\Psi_\alpha(x,y) = \sqrt{\frac{2}{w(x)}} \sum_{n=0}^{N_n} \sum_{m=1}^{N_m} c_{\alpha,\{mn\}} \sin\frac{\pi m x}{L} \cos\frac{\pi(2n+1)\,y}{w(x)} \equiv \sqrt{\frac{2}{w(x)}} \sum_{n=0}^{N_n} \psi_n(x) \cos\frac{\pi(2n+1)\,y}{w(x)}, \tag{59}$$

where the formerly defined transverse modes are (cf. Eq. (13))

$$\psi_n(x) = \sum_{m=1}^{N_m} c_{\alpha,\{mn\}} \sin\frac{\pi m x}{L}, \tag{60}$$

and the expansion coefficients are obtained by solving the eigenvector problem for the Hamiltonian matrix. In the basis (58), the matrix elements of the Hamiltonian are as follows

$$H_{pq,mn} \equiv \left\langle \phi_{pq}|\hat{H}|\phi_{mn}\right\rangle = \left(\frac{m\pi}{L}\right)^2 \delta_{p,m}\delta_{q,n} + \int_0^L h_{pq,mn}(x)\,dx, \tag{61}$$

$$h_{pq,mn}(x) = \left[\frac{h_0(q,n)}{w^2(x)} + h_2(q,n)\left(\frac{w'(x)}{w(x)}\right)^2\right]\sin\frac{\pi p x}{L}\sin\frac{\pi m x}{L} + \\ + h_1(q,n)\frac{w'(x)}{w(x)}\left(\frac{m\pi}{L}\sin\frac{\pi p x}{L}\cos\frac{\pi m x}{L} - \frac{p\pi}{L}\cos\frac{\pi p x}{L}\sin\frac{\pi m x}{L}\right), \tag{62}$$

where

$$h_0(q,n) = \pi^2(1+2n)^2\delta_{q,n}, \quad h_1(q,n) = \frac{(-1)^{n+q}(1+2n)(1+2q)}{2(n-q)(1+n+q)}(1-\delta_{q,n}), \\ h_2(q,n) = \begin{cases} \frac{(-1)^{n+q}(1+2n)(1+2q)(1+2n(1+n)+2q(1+q))}{2(n-q)^2(1+n+q)^2}, & n \neq q \\ \frac{3+\pi^2(1+2m)^2}{12}, & n = q \end{cases}. \tag{63}$$

The integration in (61) is performed numerically by digitizing the x-coordinate. Note that the above expression is explicitly symmetric. Actually, this is not obligatory, but otherwise the Hamiltonian matrix should be symmetrized like $(H + H')/2$ in order that the numerical diagonalization be stable.

The smoothness of the waveguide width profile is introduced by means of a convolution of the binary width profile (i.e. a fixed nominal width for the letters A and B) with the Gaussian kernel,

$$g(x) = \frac{1}{\sqrt{\pi}\eta a}e^{-(x/\eta a)^2}, \quad \int g(x)\,dx = 1 \tag{64}$$

where a is the single letter length ($a = 1.35\,\mu$m in the experiment reported in EPL) and the relative, dimensionless smoothness scale η is used as a fitting parameter (to the experimental data). Actually (for "historical reasons"), below we use slightly different notation for the smoothness parameter S_m (not to be confused with the notation of the Fibonacci sequences S_j), which is related to η by

$$\eta = S_m \times (1.07/8)/\sqrt{2} \approx 0.095 \times S_m \approx 0.1 S_m. \tag{65}$$

It is important to note, that we have assumed that the above smoothing procedure is generic, which is not evident at all. In particular, it is well known that Gaussian shaped scatterers have very non-generic cross section at high energies (see, e.g., Landau Vol.III). Late note: some calculation was done with an alternative smothing kernel (half-circle) and the results was nearly the same.

B. Convergence tests

The convergence tests were performed for the Fibonacci wires of different generations (the corresponding MATLAB function is calc_spectr_Fib_2D.m). The physical parameters were drawn from the experimental setting:

$$w_B = 2.04\,\mu\text{m}, w_A = 3.5\,\mu\text{m}, a = 1.35\,\mu\text{m}, \tag{66}$$

and the (now not important) exciton-photon coupling parameters E_c, E_x and Ω also given an experimental values. Different smoothness scales were considered. The parameters which control the numerical convergence of the diagonalization are the number of the transverse modes N_n, the size N_m of the sub-basis for each transverse mode, and the numerical grid parameter P defined as the number of the grid points per single letter (i.e. the letter length a in units of the lattice spacing). The later is important because the geometric potential contains various derivatives of the width $w(x)$, which change fast for sharp geometry.

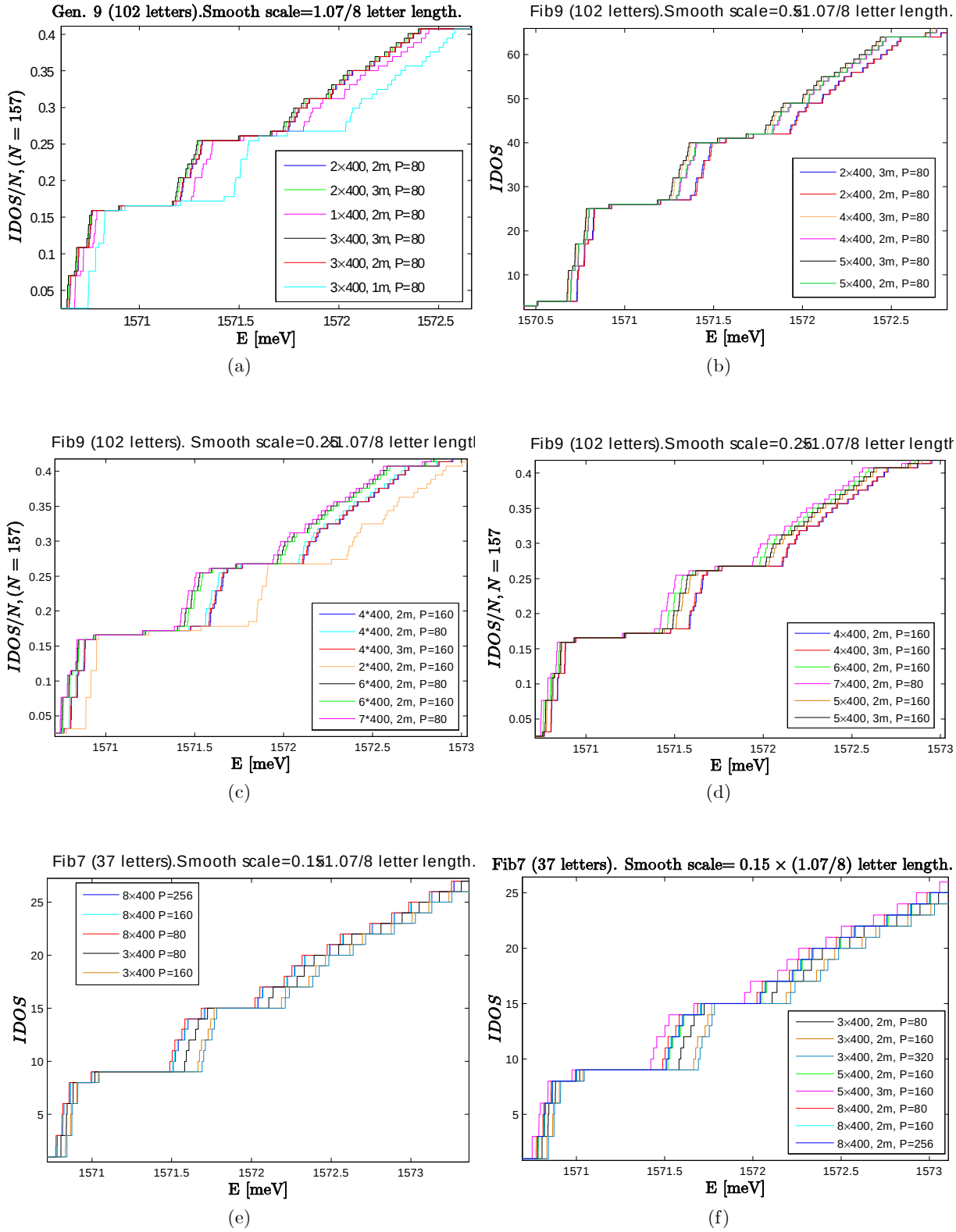

FIG. 2: Convergence tests for the 2D calucaltion of the polaritonic spectrum in a quasi-periodic system.

The numerical convergence of the 2D calculation depends strongly on the smoothness of the waveguide width geometry, as should be expected already from the general considerations given above (namely the note that the single-mode approximation becomes singular and the coupling to higher modes becomes more important for sharper geometries). Generally, it is easy to anticipate the required number of the longitudinal basis states N_m and the grid parameter P. Both should at least comply with the scale of the the variation of the width $w(x)$ in terms of the smallest wavelength and the grid spacing respectively (this statement is in agreement with the numerics below). It is somewhat harder to predict the required number of the transverse modes N_n. This is because by the constructions they are already build to follow the waveguide boundary, and the requirement should come from the anticipation of the variation scale of the evanescent field at the corners in y-direction. One could assume (formally/blindly) that the latter is of the same order as the scale of the smoothness in x-direction, but the numerics below indicates that the requirement on N_n is much softer (as long as the eigenspectrum is concerned).

The convergence tests and requirements are summarized for the relevant smoothness scales in Fig. 2 presenting the eigenspectrum for different settings. Each panel represents a given smoothness scale. The smoothness scale is indicated in the panel titles (it is in a somewhat weird form $S_m \times (1.07/8)$ of the letter width a, where S_m is some number, which is because of the "historical reason: the value 1.07/8 was used to tune the 1D effective calculation into the experimental data). In the legends are given the longitudinal basis size N_m as $\# \times 400$, the number of the transverse modes N_m as $\#m$ (where $\# = N_m$) and the grid parameter P. Panels Fig. 2(a-d) correspond to the "Fib9" (in the French notation), which means almost the Fibonacci sequence S_{11} (see Appendix A) with paddings of 7 and 6 wide-width (A) letters, which is overall 102 letter long. Respectively, "Fib7" in Fig. 2(e,f) is nearly S_9, but with padding of 2 A-letters, overly 37 letter long. The shorter than experimental system had to be taken in order to overcome numerical memory limitations in MATLAB encountered on the way to convergence (the original code is not optimized to face this problem). The essential convergence conditions are not expected to be dependent on the system length, but **it should be kept in mind that same number of the longitudinal modes N_m means different smallest wavelengths for different systems** (therefore, e.g., a smaller basis is required for Fib7 than for Fib9). This note, of course, is not relevant to the other parameters N_n and P. The convergence is said to be achieved when the IDOS curve does not change significantly upon the increase of one of the three parameters.

Let us summarize the main conclusions from the convergence examination:

1. The required grid spacing is such that the smoothness ($S_m \times (1.07/8) \times a$) length contains about $5 \div 10$ grid points [this is because the geometric potential is comprised of the derivatives of $w(x)$]. So, for S_m up to 0.5, $P = 80$ were (more than) enough, while higher values are required for sharper geometry. Namely, for $S_m = 1$, the smoothness length is $\lambda \sim 1/8$ so that required $P \sim 10/\lambda = 80$ points per letter.

2. The required size of the "longitudinal" basis N_m is such that the smallest wavelength is of the order of the smoothness length. E.g., for $S_m = 1$, the wavelength is $\lambda \sim 1/8$, so that the corresponding $N_m \sim 102/\lambda \approx 800$, where 102 is the system length. Indeed, Fig. 2(a) shows that the convergence is practically achieved for $N_m = 2 \times 400$, while for $S_m = 0.5$ in Fig. 2(a) - for the twice larger $N_m = 4 \times 400$.

3. As noted above, the required number of the transverse modes N_n is hard to explain in elementary and intuitive terms (at least to me presently). It turns out that the importance of the included higher mode decreases with the mode order (note that we look only on the lower part of the spectrum, where the modes above the lowest one are not propagating (i.e., give only an evanescent contribution). As a rule, there is a huge difference in the spectrum when going from one to two modes (shown only in panel (a)), - also for smoother structures not reported here (e.g. for $S_m = 2$, - see also the next subsection). Much more moderate change is found when going from two to three transverse modes. Expectably, this change increases for sharper geometries. Note, that the "mutual" convergence in $\{N_n, N_m, P\}$ was not reached for $S_m = 0.25$ in panels (c,d) [for the memory issues with long Fib9], but it was for sharper $S_m = 0.15$ (for shorter Fib7). To appreciate the effect of the 3rd mode, pay attention to the corresponding shift of the second sub-band, which is about 0.04 meV and 0.1 meV for $S_m = 1$ and $S_m = 0.15$ respectively, Fig. 2(a,f).

4. The effect of adding the 4th mode to the calculation was not examined. Based on the effect of the 3rd mode, for the considered smoothnesses it is expected to be negligible. For yet sharper geometries it should be necessary. The latter does not mean that the lower part of the spectrum would change significantly for increased sharpness, but only pertains to the calculation procedure (it is plausible that some alternative calculation scheme would be more optimal for the ultimately sharp step-wise geometry). Indeed, physically one would not expect any effect of the sharpness variation when its scale is already much smaller than the relevant wavelengths.

5. Regarding the "direction" of the change in the spectrum induced by the variation of the three parameters:

   - increasing P "enhances" the band structure (wide gaps, narrower bands) (since it restores the true amplitude of the geometric potential),

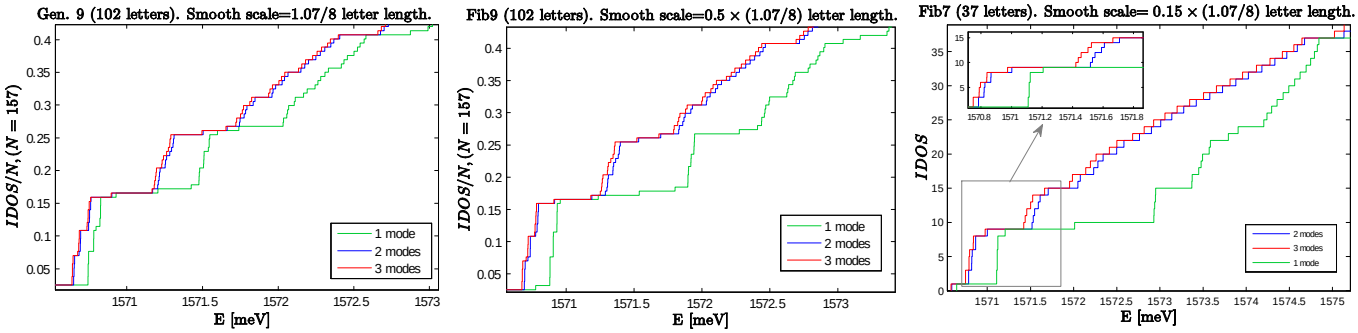

(a) (b) (c)

FIG. 3: The effect of the mode coupling.

- increasing N_m and N_n "moderates" the band structure (narrower gaps, wider bands), - since in effect it moderated the effective 1D potential.

6. As a clarifying (though evident) comment to the above points, it should be emphasized that convergence in one of the three parameters does not mean yet convergence to the physical solution. E.g., a solution can be convergent in N_n and P for a chosen N_n, while increasing N_n would further modify it.

C. Importance of mode coupling

In the previous subsection the technical aspect of the convergence was at the focus. A more important/interesting physical question is how much the mode coupling matters for the lower part of the spectrum considered here (see also the item (4) above). This question has two aspects (related, but whose relation is not straightforward):

- what is the relative weight of the higher transverse modes in the exact eigenmodes, and
- how much is the calculated spectrum affected by taking into the account (or neglecting) the mode coupling.

Regarding the first point (no figures at present), it was found for the smoothness $S_m = 1$ that the relative weight of the second mode is very small (locally at most about 10^{-2} in intensity [**???-check this**]) and it is concentrated in x at the steps of the width $w(x)$. **To be completed ...**

The second point is addressed in Fig. 3 by comparing energy spectra calculated using different number of the transverse modes for three values of the smoothness scale $S_m \times (1.07/8) \times a$, $S_m = 1, 0.5, 0.15$. For each given number of the transverse modes N_n the convergence has been achieved in other two parameters N_m and P. Fig. 3 demonstrates more neatly the conclusion already states above. Namely, in the considered range of the smoothness scale, there is a drastic effect of adding 2nd mode to the 1st one, while adding 3rd mode have a moderate, but finite effect on the lower part of the eigenspectrum. To appreciate the effect of the 3rd mode, consider the corresponding shift of the second sub-band, which is about 0.04 meV and 0.1 meV for $S_m = 1$ and $S_m = 0.15$ respectively.

D. Dependence of the spectrum on the smoothness of the waveguide geometry

In this subsection the effect of the of the smoothness/sharpness of the waveguide geometry is singled out. The eigenmode spectrum for the Fibonacci system Fib9 (sequence S_{11}) is shown in Fig. 4 for several values of the smoothness parameter indicated in the legends. For the first three data series the complete convergence has been achieved (3-mode calculation), while for the other two the result is expected to be "relatively" close to convergence (namely, it is pretty convergent for the given here 2-mode calculation, while adding the third mode would shift it by finite but moderate amount to the left, deducible from Fig. 3, - the 2^{nd} sub-band of the green curve shifts left by at most 0.1 meV, - see previous subsection). Presumably, the lack of the convergence of the last two series could explain the seemingly non-uniform shift of the spectrum as a function of the smoothness parameter.

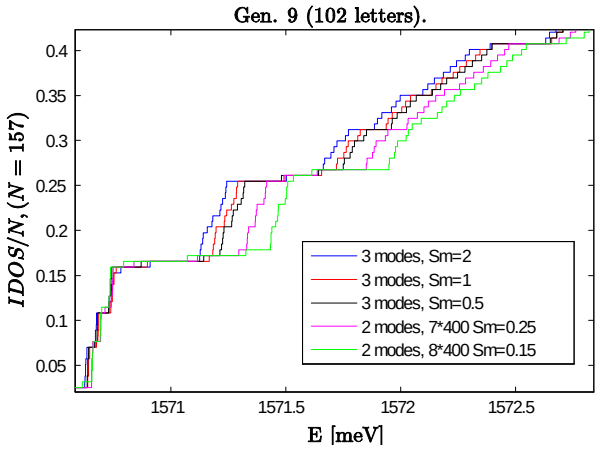

FIG. 4: The effect of the smoothness of the waveguide geometry.

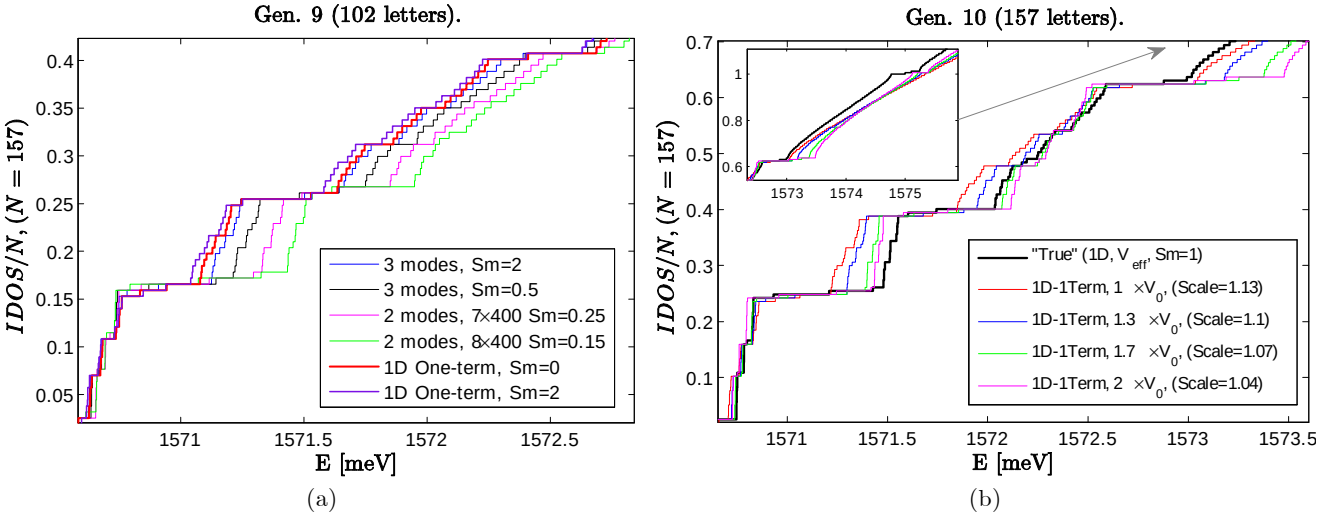

(a) (b)

FIG. 5: 1D - one term approximation: (a) Comparison to the 2D calculation for the different degrees of the waveguide geometry smoothness. 1D calculcation is done for the unsmoothed (step-wise) profile (red curve), and for the smoothness scale $2\times(1.07/8)$ (perple curve). The two spectra differ a little, - in contrast to the correct 2D result. (b) 1D-one term approximation "tuned" by enhancing the geometric potential like $x \times V_0$ and, then, scaling the energy scale of the spectrum, as indicated in the legends. This is compared to the "true" result of the effective 1D calculcation (black), which agrees well with the experiment. In spite of the certainly exhagerated strength of the geometric potential (in the extreme case), the 1D-one term approximation fails to reproduce quantiatively the correct spectrum (e.g., in terms of the relative position and width of the second and the third main sub-bands).

Even assuming that the "sharpest" $S_m = 0.15$ green curve in Fig. 4(a) should in fact be in place of the magenta one (and the latter one somewhere "in between"), these results show clearly the non-negligible effect of the sharpness of the geometry in the considered regimes. Nevertheless, it seems plausible that further increase of the sharpness (smaller smoothness) would not affect the spectrum significantly (provided the calculation is made converging by taking into the account the higher transverse modes). The later are important to satisfy the zero boundary conditions at the sharp corners, but do not change much the eigenenergies. On the other hand, disregarding them causes incorrect treatment of the lower transverse mode, which results in an incorrect spectrum overly sensitive to the sharpness (one can say that the higher modes serve as a "lubricant" for the lower ones at the sharp corners of the waveguide). To summarize, the smoothness scales considered in Fig. 4(a) do have significant effect on the eigenspectrum since they are comparable to the relevant longitudinal wavelengths.

E. 2D vs 1D single-mode adiabatic approximation

The conclusion of the last paragraph in the previous subsection could suggest that the most simple 1D calculation with the 1^{st} term only kept in the potential in (16), i.e. $\pi^2/w^2(x)$, would actually be better then using the complete $V_{eff}(x)$ for the lowest mode,

$$V_{eff}(x) = \frac{\pi^2}{w^2(x)} + \frac{\pi^2+3}{12}\left(\frac{w'(x)}{w(x)}\right)^2, \tag{67}$$

(such approximation seems to be called an "adiabatic approximation", since it is valid for slow variation of the width $w(x)$). A possible argumentation in favour of such a situation is that the entire expansion is rather singular, and many terms are needed to sum up and produce eventually a rather moderate effect of the sharp corners, while keeping only a small fraction of them would only spoil the result. To clarify this point the calculation was done in a single mode approximation (i.e. 1D) with only the 1^{st} term kept in the potential in (16). Fig. 5(a) shows that such approximation (a) does not reproduce quantitatively the 2D calculation, and in particular (b) is almost insensitive to the smoothness of the waveguide geometry, i.e. nearly same spectrum for the relatively strong smoothing (purple) and none at all (red).

The quantitative disagreement between this 1D approximation and the 2D calculation consists not only in different energy scale, but in the shape of the spectrum (i.e. the relation between the band and the gap widths). After some numerous attempts (in the beginning of this work) it turned out that this disagreement could not be corrected by varying the effective potential strength and the exciton-photon coupling parameters. Moreover this 1D approximation eliminates the gap at about $E = 1575\,\text{meV}$ present in the experiment and the more exact calculations (not shown in Fig. 4). This is for the trivial reason that the rectangular potential barriers (or nearly so if smoothed) of the letter B are transparent (nearly transparent) at this energy (i.e. the resonant transition), which is a coincidence of the gap position and the letter length (in the language of the Bragg peaks: zero of the *sinc*-function coincides with the Bragg peak). This transparency is removed if the 2^{nd} term in the effective potential (67) is retained. These numerous attempts to make out with the 1D-one term approximation are described in the memo document "*Insufficiency of the quadratic approximation.pptx*" (update the file name if required). They are not summarized here since "iterations" of the treatment of the exciton-photon coupling there is questionable. Essentially the same calculation is repeated in Fig. 5(b) [using the correct coupling procedure described above]. It represents failing attempts to tune the 1D-one term approximation into the "experimental data" (black) by first manually scaling the geometric potential $V_0 \equiv \pi^2/w^2(x)$ and, then, changing the energy scale of the obtained spectrum (see legends) [the idea was to obtain first the correct shape of the spectrum and, then, to tune the energy scale by varying the exciton-photon coupling]. The agreement could not be achieved even playing with a broad range of these parameters. Note that the gap near $E = 1575\,\text{meV}$ does opens eventually, Fig. 5(b,inset), which could be a higher order effect (in terms of the PT), or the numerical artifact - this point was not examined.

The bottom-line conclusion is that the 1D-one term approximation is

(a) not sufficient to describe quantitatively the experimental spectrum, and

(b) not appropriate if the waveguide width variation is not slow compared to the relevant longitudinal wavelength (if required, some straightforward quantitative criterion can be deduced from the relative strength of the terms in the effective 1D potential in (16)).

F. 2D vs 1D single-mode effective potential approximation

Here the 1D single-mode approximation using the effective potential (67) is compared to the full 2D calculation. This approximation means neglecting any coupling between the lowest transverse mode the higher ones, i.e. truncating the coupled equation hierarchy (14) to $m = 0$. This is the approximation used in the paper on the Fibonacci wire spectrum and described shortly in its supplementary materials. Also, this is the same as the 1-mode calculation given sometimes above.

Already when writing the supplementary material to the paper the comparison of this 1D approximation to the full 2D calculation was made and it was clear that the results differ a lot for a given smoothness scale of the waveguide geometry (see. Section VI D). On the other hand, and quite surprisingly, it was found numerically that the spectra calculated in those two ways can be made very similar if the waveguide smoothness is reduced for the 2D calculation. This observation was presented in the supplementary of the paper, and the (apologetic) argument was stated that the

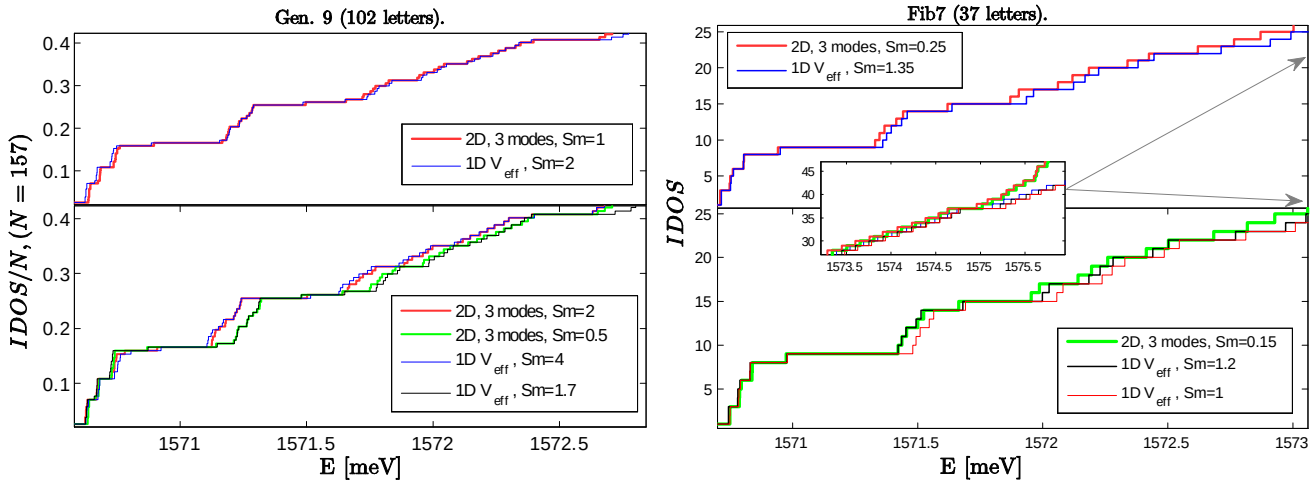

(a) (b)

FIG. 6: 1D single-mode effective approximation compared to the full 2D calculation fro different degree of the waveguide boundary smoothness.

smoothness scale was anyway used as a phenomenological parameter to fit the experiment (therefore, what we have done using the 1D calculation was OK after all).

Fig. 6 demonstrates the "matching" between the full 2D and the 1D single-mode effective potential approximation. All the results of the 2D calculation presented in Fig. 6 are converging (using 3 modes and taking shorter wire if required by the memory limitations). Thus, they are considered as true spectra. In panel (a) the system is Fib9 (i.e. S_{11}) 102 letters long, while in panel (b) it is Fib7 (S_9) 37 letters long. As already noted above, the difference in the wire length from that described in the letter to EPL is not expected to affect the issue under the present consideration (although, evidently, the finer details of the calculated spectrum are not present, but they are not presently experimentally detectable anyway). The legends in Fig. 6 provide the details of the calculation model and, in particular, the smoothness parameter S_m, such that the smoothness length is

$$\text{smoothness length}=S_m \times (1.07/8) \times a, \tag{68}$$

where a is the single letter length. Fig. 6 demonstrates that playing with the value of S_m one can tune the 1D result into the exact 2D IDOS curve, - at least in the considered range of S_m for 2D (I believe that any S_m used for 2D can be matched by some 1D calculation, but not wise versa). The "smoothness matching" between the 2D and the 1D calculations is summarized in the following table:

$S_m\,(2D)$	2	1	0.5	0.25	0.15
$S_m\,(1D)$	4	2	1.7	1.35	1.2

(69)

It shows that the 1D single-mode effective potential approximation greatly over-estimates the effect of the waveguide sharpness ("stronger effect" means here wider gaps and narrower bands - "more fractality"). Note that this false sensitivity increases for smaller S_m. This fact only underlines the former statement that for sharp structure the single-mode truncation of (14) becomes singular and higher modes have to be included. In the elementary terms, this is related to the quadratic dependence of the effective potential (67) on the logarithmic derivative of $w\,(x)$, which is equivalent to the δ-function squared (impenetrable).

Finally, concerning the experiment and the related EPL, the single-mode effective potential calculation there have used $S_m = 1$. According to Fig. 6(b), it is in fact still a bit "more drastic" than the 2D with $S_m = 0.15$, which is sharper than that reported $\eta = 0.02$ in Fig. 1 of the related supplement, namely $\eta = 0.02$ versus $\eta = S_m\,(1.07/8)\,/\sqrt{2} = 0.014$ (the difference, however, may also be compensated by changing the energy scale, e.g. by fitting the exciton-photon parameters and the effective refractive index of the Bragg cavity).

VII. WHAT IS MEASURED IN THE EXPERIMENT

In contrast to the numerically constructed eigenfunction or spectral function maps, in the experiment a wave packet is measured. This means that the eigenmodes are in certain coherent linear superposition. Besides, spectrometry of the measured luminescence has a finite resolution, as well as the so called eigenmodes also have a finite width. We can try to write the measured intensity at energy E and position x as

$$I(E,x)=\left|\int\rho(E')\,g(E-E')\,\alpha(E')\,\psi_{E'}(x)\,e^{i\theta(E')}dE'\right|^2, \tag{70}$$

where $\alpha(E')$ is the (real) expansion coefficient and $\theta(E')$ describes the phase of the eigenstate $\psi(x)$ (to fix explicitly the relative phase between different states), and dimensionless real-valued window function $g(E-E')$ describes the spectral resolution of the measurement (or/and the [uniform] width of the modes). Expanding the above gives

$$I(E,x)=\int\rho(E'')\,\rho(E')\,g(E-E'')\,g(E-E')\,\alpha(E'')\,\psi^*_{E''}(x)\,\alpha(E')\,\psi_{E'}(x)\,e^{i\theta(E')-i\theta(E'')}dE'dE''. \tag{71}$$

If we integrate over x, assuming the orthogonality $\rho(E'')\,\langle\psi^*_{E''},\psi_{E'}\rangle=\delta(E''-E')$, then

$$I(E,x)=\int I(E,x)\,dx=\int\rho(E')\,|\alpha(E')|^2\,g^2(E-E')\,e^{i\theta(E')-i\theta(E')}dE'=|\alpha(E)|^2\,\rho(E)\,\Delta E, \tag{72}$$

where ΔE characterizes the width of the window function $g^2(E-E')$. Thus, the relative phase is not important for this measurement.

If we want both the energy and the position resolved measurement, then ... (???)

VIII. NUMERICAL RESULTS AND COMPARISON TO THE EXPERIMENT

For the model defined above we have calculated the eigenenergies and eigenfunctions as described in Appendix A. Below we present the integrated density of states and the visualization maps of the corresponding eigenfunctions in the position and the momentum spaces. It should be stressed that no attempt to calculate the actual (experimental) occupation of the eigenstates was made so far, and the maps below represent the normalized eigenfunction intensities with equal weight.

A. Integrated density of states (IDOS)

The IDOS was calculated as explained in Appendix A, and the results are shown in Fig. 7.

B. Eigenfunction maps

The eigenfunction are calculated as explained in Appendix A. As mentioned above, presently we do not calculate the occupation of the modes in the experimental process, but simply represent the mode map visualization in the position-energy axes.

Visualization method: grossly, the energy axis is digitized on the scale of $5\times10^{-2}E_R$. Then, each energy window is assigned the value of the sum of the intensities $|\psi(x)|^2$ of the eigenfunctions belonging to this window (actually, the Gaussian weight function is used). This is done position-wise, which eventually produces the position-energy maps shown in Fig. 8. The intensity is represented in the linear (not logarithmic) colormap scale.

As expected, and in accord with the IDOS plots in Fig. 7, the gaps become wider and the bands become narrower for higher value of V_0/E_R. It should be noted that the individual modes do not extend uniformly over the system length, as could be misunderstood from the maps in Fig. 7. Rather, they are peaked in certain segments of the system. However, usually there are several adjacent (in energy) modes, which, when combined incoherently by intensities, together produce a uniform (albeit modulated) pattern over the system length. This is what we see in Fig. 7.

Finally, there are some edge-gap states, due to the padding with the uniform sections $AAAAAA$'s in (2).

It seems that the calculations for the larger values of $\tilde{V}_0=\frac{V_0}{E_R}=\frac{1.5}{1.15},\frac{2}{1.15}$ fit the experiment better than for the "nominal" value $\tilde{V}_0=\frac{1}{1.15}$, - both in terms of the ratios between the band and gap widths, and in terms of the

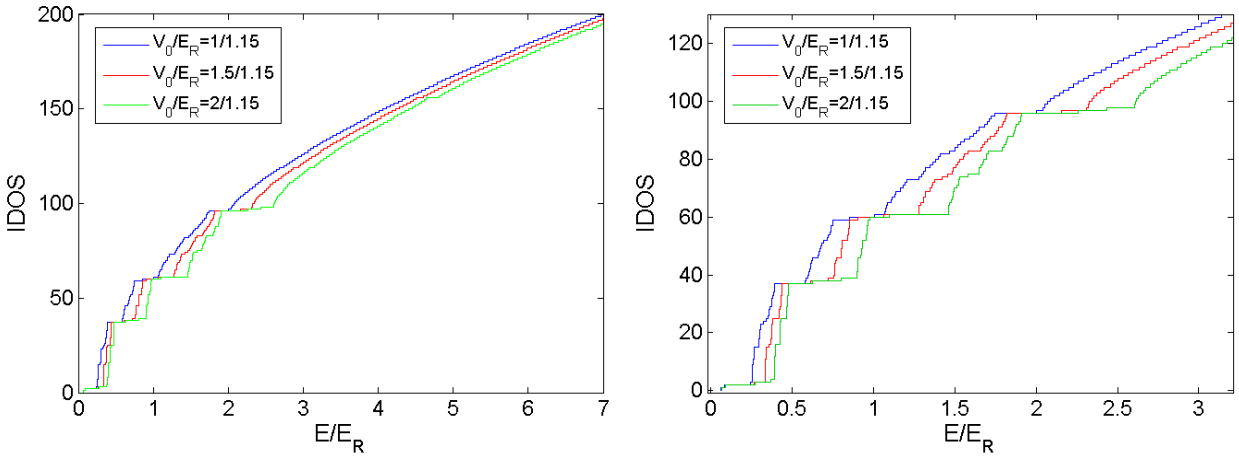

FIG. 7: Integrated density of states (IDOS), in units of the number of states, for three different values of V_0/E_R (see legends). Panel (b) give zoom of the plot in (a).

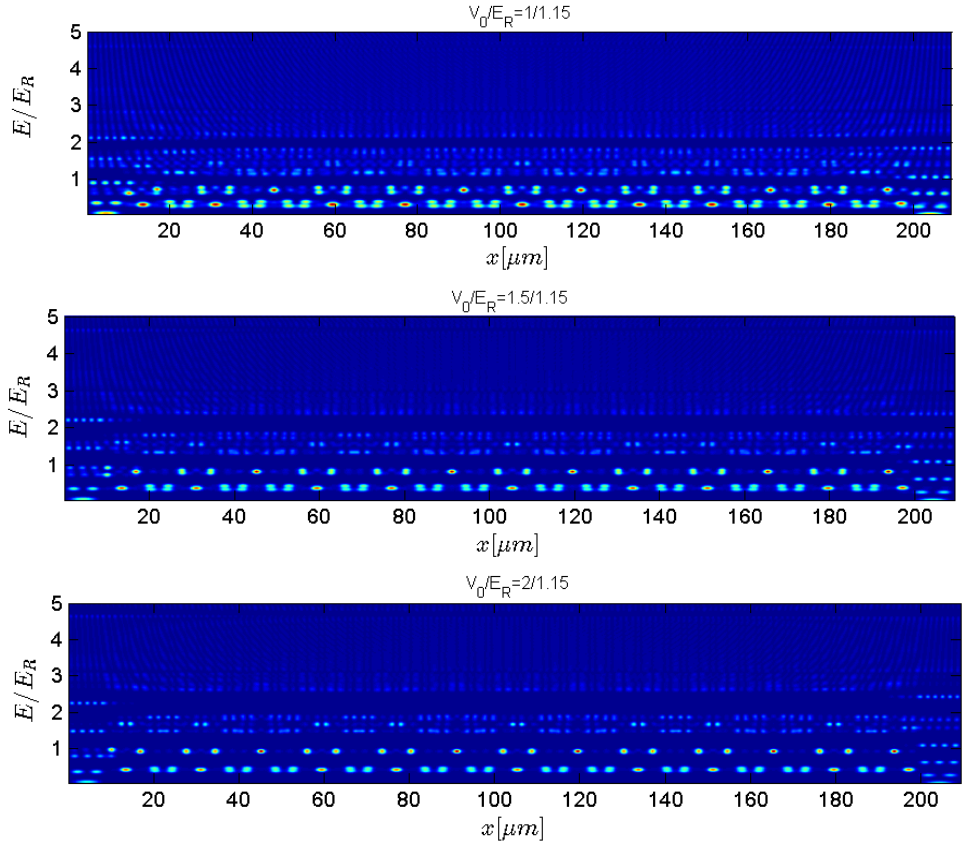

FIG. 8: Eigenfunction intensity maps in the position-energy axes for three different values of V_0/E_R (see titles). The gaps become wider and the bands become narrower for higher value of V_0/E_R.

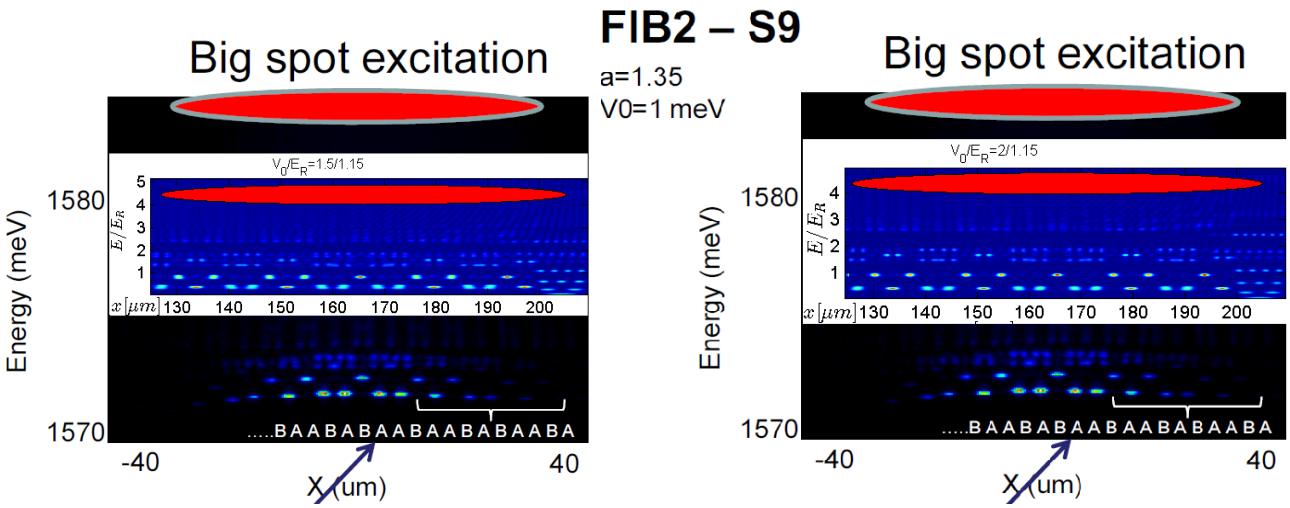

(b) $V_0/E_R = 1.5/1.15$ (b) $V_0/E_R = 2/1.15$

FIG. 9: Eigenfunction intensity maps in the position-energy axes for $V_0/E_R = 1.5/1.5, 2/1.15$ compared to the experiment for FIB2.

eigenmode patterns. To make the comparison more clear, the maps in Fig. 7 are zoomed and brought in-scale on top of the experimental figure cropped from the presentation. This is shown in Fig. 9. Pay attention that the energy scale of the numerical data is in units of E_R. To make the final comparison, we need to know the relevant values of V_0 and E_R.

C. Spectral function

An analogue of the spectral function, $a\,(E, k)$, is constructed by performing the Fourier transform of each eigenfunction, discussed above. Then, the intensity of the Fourier transforms is visualized in the momentum-energy axes in the precisely the same way as described above for the position-energy presentation of the eigenfunctions.

The result is presented in Fig. 10. The intensity of the numerical results is represented in the linear (not logarithmic) colormap scale.

APPENDIX A: CALCULATION OF EIGENENERGIES AND EIGENFUNCTIONS

The eigenenergies and the eigenfunctions can be found either by the diagonalization of the Hamiltonian calculated in the relevant subspace of the using the basis of the eigenfunctions of the uniform system (i.e. $\sin kx$), or using the zero-counting theorem. The former is convenient for relatively short systems (in terms of the number of the letters). The latter allows to treat much longer systems and seems to allow better accuracy. In the present context, both methods can be used and give nearly the same results (this was verified). The zero-counting method is described below.

APPENDIX B: TEST (CALIBRATION) CALCULATION FOR THE PERIODIC SYSTEM

In order to test our calculation, the density of states and the spectral function was calculated for the periodic system, $...ABABA...$, and compared to the experimental results given in Fig 1(b) in [1]. The comparison is given in Fig. **??**, which shows that the position of the gap is calculated correctly. However, the energy scale in the numerical result is larger by about the factor 1.5 in respect to the measured one. Supposedly, this results from the incorrect calibration of the recoil energy by the same factor (probably, because of the heavier actual mass of the polariton?).

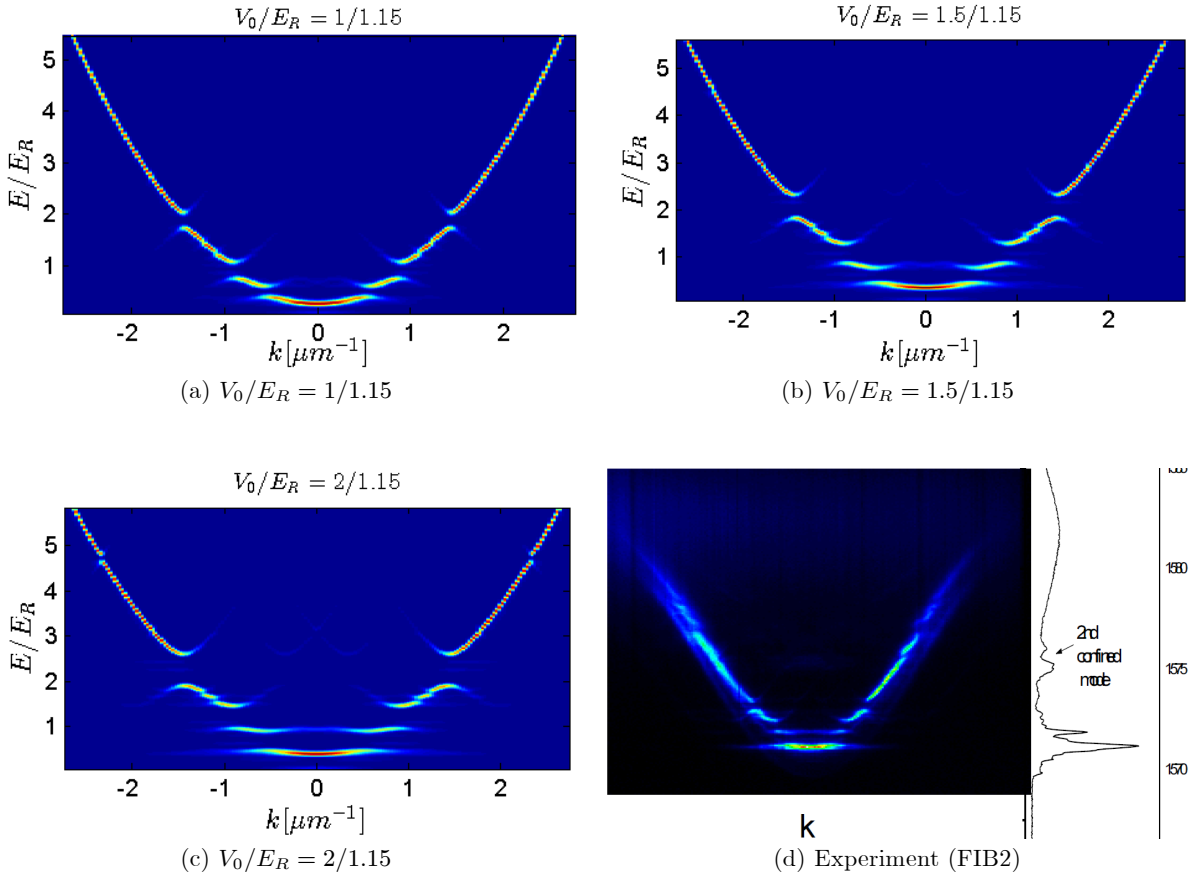

(a) $V_0/E_R = 1/1.15$ (b) $V_0/E_R = 1.5/1.15$

(c) $V_0/E_R = 2/1.15$ (d) Experiment (FIB2)

FIG. 10: Spectral function intensity maps in the momentum-energy axes for three different values of V_0/E_R compared to the experimental result for FIB2 from the presentation.

APPENDIX A: REORDERING OF THE EXPERIMENTAL FIBONACCI WIRE AS A SINGLE S_n

For some reason, the (first) experimental system was constructed as a concatenation

$$[S_1, S_2, ..., S_{10}]\,, \tag{A1}$$

where each $S_{j\geq 3} = [S_{j-2}S_{j-1}]$, and $S_1 = B$, $S_2 = A$. It turns out that such a concatenation can be written as an almost single S_n:

$$S_{m+2} = \begin{bmatrix} [[S_2]\,S_1, S_2, ..., S_m] & \text{even } m \\ [S_1\,[S_2]\,, S_2, ..., S_m] & \text{odd } m \end{bmatrix}. \tag{A2}$$

For even m the equivalence is complete, because the quasiperiodic part of the wire was padded with sections equal in width to the A-letter.

The (non-elegant) proff is as follows. For the even m, e.g. $m = 10$

$$\underbrace{\underbrace{\underbrace{[S_2]}_{S_4}\underbrace{S_1S_2}_{S_5}\underbrace{S_3S_4}_{S_7}}_{S_6S_7=S_8}\underbrace{S_5S_6}_{S_9}\underbrace{S_7S_8}_{S_{11}}\underbrace{S_9S_{10}}}_{S_{10}S_{11}=S_{12}} = S_{12}, \tag{A3}$$

from which the general rule follos by deduction. For the odd m, e.g. $m = 5$

$$\underbrace{S_1\,[S_2]}_{S_3}\underbrace{S_2S_3}_{S_4}\underbrace{S_4S_5}_{S_6} = S_5S_6 = S_7. \tag{A4}$$

APPENDIX B: CALCULATION OF $\hat{H}_{01}(x)\hat{H}_{10}(x)$

$$\hat{H}_{01}(x)=-\frac{3}{4}\left[\left(\frac{w''(x)}{w(x)}+2\frac{w'(x)}{w(x)}\frac{d}{dx}\right)+\frac{3}{2}\left(\frac{w'(x)}{w(x)}\right)^2\right], \tag{B1}$$

$$\hat{H}_{10}(x)=-\frac{3}{4}\left[-\left(\frac{w''(x)}{w(x)}+2\frac{w'(x)}{w(x)}\frac{d}{dx}\right)+\frac{7}{2}\left(\frac{w'(x)}{w(x)}\right)^2\right], \tag{B2}$$

so that

$$\begin{aligned}\hat{H}_{01}(x)\hat{H}_{10}(x)&=\tfrac{9}{16}\left[\tfrac{3}{2}\left(\tfrac{w'(x)}{w(x)}\right)^2+\left(\tfrac{w''(x)}{w(x)}+2\tfrac{w'(x)}{w(x)}\tfrac{d}{dx}\right)\right]\left[\tfrac{7}{2}\left(\tfrac{w'(x)}{w(x)}\right)^2-\left(\tfrac{w''(x)}{w(x)}+2\tfrac{w'(x)}{w(x)}\tfrac{d}{dx}\right)\right]\\&=\tfrac{9}{16}\left\{\tfrac{21}{4}\left(\tfrac{w'(x)}{w(x)}\right)^4-\left(\tfrac{w''(x)}{w(x)}+2\tfrac{w'(x)}{w(x)}\tfrac{d}{dx}\right)^2+\tfrac{7}{2}\left(\tfrac{w''(x)}{w(x)}+2\tfrac{w'(x)}{w(x)}\tfrac{d}{dx}\right)\left(\tfrac{w'(x)}{w(x)}\right)^2-\tfrac{3}{2}\left(\tfrac{w'(x)}{w(x)}\right)^2\left(\tfrac{w''(x)}{w(x)}+2\tfrac{w'(x)}{w(x)}\tfrac{d}{dx}\right)\right\}\\&=\tfrac{9}{16}\left\{\tfrac{21}{4}\left(\tfrac{w'(x)}{w(x)}\right)^4+2\tfrac{w''(x)}{w(x)}\left(\tfrac{w'(x)}{w(x)}\right)^2-\left(\tfrac{w''(x)}{w(x)}+2\tfrac{w'(x)}{w(x)}\tfrac{d}{dx}\right)^2+14\left(\left(\tfrac{w'(x)}{w(x)}\right)^2\tfrac{w''(x)}{w(x)}-\left(\tfrac{w'(x)}{w(x)}\right)^4\right)+4\left(\tfrac{w'(x)}{w(x)}\right)^3\tfrac{d}{dx}\right\}\\&=\tfrac{9}{16}\left\{-\tfrac{35}{4}\left(\tfrac{w'(x)}{w(x)}\right)^4+16\tfrac{w''(x)}{w(x)}\left(\tfrac{w'(x)}{w(x)}\right)^2+4\left(\tfrac{w'(x)}{w(x)}\right)^2\tfrac{w'(x)}{w(x)}\tfrac{d}{dx}-\left(\tfrac{w''(x)}{w(x)}+2\tfrac{w'(x)}{w(x)}\tfrac{d}{dx}\right)^2\right\}.\end{aligned}$$

The operator squared in the above expression is

$$\begin{aligned}\left(\tfrac{w''(x)}{w(x)}+2\tfrac{w'(x)}{w(x)}\tfrac{d}{dx}\right)^2&=\left(\tfrac{w''(x)}{w(x)}\right)^2+2\tfrac{w''(x)}{w(x)}\tfrac{w'(x)}{w(x)}\tfrac{d}{dx}+2\tfrac{w'(x)}{w(x)}\tfrac{d}{dx}\tfrac{w''(x)}{w(x)}+4\tfrac{w'(x)}{w(x)}\tfrac{d}{dx}\tfrac{w'(x)}{w(x)}\tfrac{d}{dx}\\&=\left(\tfrac{w''(x)}{w(x)}\right)^2+2\tfrac{w'(x)}{w(x)}\left(\tfrac{w''(x)}{w(x)}\right)'+4\tfrac{w''(x)}{w(x)}\tfrac{w'(x)}{w(x)}\tfrac{d}{dx}+4\tfrac{w'(x)}{w(x)}\left(\tfrac{w''(x)}{w(x)}-\left(\tfrac{w'(x)}{w(x)}\right)^2\right)\tfrac{d}{dx}+4\left(\tfrac{w'(x)}{w(x)}\right)^2\tfrac{d^2}{dx^2}\\&=\left(\tfrac{w''(x)}{w(x)}\right)^2+2\left(\tfrac{w'(x)}{w(x)}\tfrac{w'''(x)}{w(x)}-\tfrac{w''(x)}{w(x)}\left(\tfrac{w'(x)}{w(x)}\right)^2\right)+4\tfrac{w'(x)}{w(x)}\left(2\tfrac{w''(x)}{w(x)}-\left(\tfrac{w'(x)}{w(x)}\right)^2\right)\tfrac{d}{dx}+4\left(\tfrac{w'(x)}{w(x)}\right)^2\tfrac{d^2}{dx^2}.\end{aligned}$$

Finally (checked with Mathematica)

$$\begin{aligned}\hat{H}_{01}(x)\hat{H}_{10}(x)=\frac{9}{16}&\left\{-\frac{35}{4}\left(\frac{w'(x)}{w(x)}\right)^4+18\frac{w''(x)}{w(x)}\left(\frac{w'(x)}{w(x)}\right)^2-\left(\frac{w''(x)}{w(x)}\right)^2-2\frac{w'(x)}{w(x)}\frac{w'''(x)}{w(x)}\right\}-\\&-\frac{9}{4}\left\{2\left(\frac{w'(x)}{w(x)}\frac{w''(x)}{w(x)}-\left(\frac{w'(x)}{w(x)}\right)^3\right)\frac{d}{dx}+\left(\frac{w'(x)}{w(x)}\right)^2\frac{d^2}{dx^2}\right\}.\end{aligned} \tag{B3}$$

The expression in the parentheses on the second line above may also be rewritten symmetrically as

$$\frac{d}{dx}\left(\frac{w'(x)}{w(x)}\right)^2\frac{d}{dx}, \tag{B4}$$

so that $\hat{H}_{01}(x)\hat{H}_{10}(x)$ becomes

$$\hat{H}_{01}(x)\hat{H}_{10}(x)=\frac{9}{16}\left\{-\frac{35}{4}\left(\frac{w'(x)}{w(x)}\right)^4+18\frac{w''(x)}{w(x)}\left(\frac{w'(x)}{w(x)}\right)^2-\left(\frac{w''(x)}{w(x)}\right)^2-2\frac{w'(x)}{w(x)}\frac{w'''(x)}{w(x)}-4\frac{d}{dx}\left(\frac{w'(x)}{w(x)}\right)^2\frac{d}{dx}\right\}. \tag{B5}$$

APPENDIX C: WAVE FUNCTION TRANSFORMATION $\psi_0(x)=f(x)\phi(x)$

One may wish to have in the effective 1D Schrodinger equation the position dependent factor in front of the second derivative instead of the canonical form as in (31). To do so, we define the transformation

$$\psi_0(x)=f(x)\phi(x), \tag{C1}$$

and look for $f(x)$ such that

$$\begin{aligned}\frac{d}{dx}\left[1-\frac{9}{4E_0}\left(\frac{w'(x)}{w(x)}\right)^2\right]\frac{d}{dx}\psi_0(x)&=\frac{d}{dx}\left[1-\frac{9}{4E_0}\left(\frac{w'(x)}{w(x)}\right)^2\right](f'\phi+f\phi')\\&=-\left[\frac{9}{4E_0}\left(\frac{w'(x)}{w(x)}\right)^2\right]'(f'\phi+f\phi')+\left[1-\frac{9}{4E_0}\left(\frac{w'(x)}{w(x)}\right)^2\right](f''\phi+2f'\phi'+f\phi'')\end{aligned} \tag{C2}$$

does not contain the first derivative of $\phi(x)$. This yields

$$-\left[\frac{9}{4E_0}\left(\frac{w'(x)}{w(x)}\right)^2\right]' f+\left(1-\frac{9}{4E_0}\left(\frac{w'(x)}{w(x)}\right)^2\right)2f'=0, \tag{C3}$$

from which

$$\frac{f'}{f}=-\frac{1}{2}\frac{\left[1-\frac{9}{4E_0}\left(\frac{w'(x)}{w(x)}\right)^2\right]'}{\left(1-\frac{9}{4E_0}\left(\frac{w'(x)}{w(x)}\right)^2\right)}, \tag{C4}$$

I.e., choosing zero free integration constant and assuming that the denominator does is positive,

$$\ln f=\ln\left(1-\frac{9}{4E_0}\left(\frac{w'(x)}{w(x)}\right)^2\right)^{-1/2}\rightarrow f=\frac{1}{\sqrt{1-\frac{9}{4E_0}\left(\frac{w'(x)}{w(x)}\right)^2}}. \tag{C5}$$

With this $f(x)$ we have

$$\begin{aligned}
-\frac{d}{dx}\left[1-\frac{9}{4E_0}\left(\frac{w'(x)}{w(x)}\right)^2\right]\frac{d}{dx}\psi_0(x)&=-\frac{d}{dx}\frac{1}{f^2}\frac{d}{dx}f\phi=-\frac{d}{dx}\frac{1}{f^2}\left(f'\phi+f\phi'\right)=-\frac{d}{dx}\left(\frac{f'}{f^2}\phi+\frac{1}{f}\phi'\right)\\
&=-\frac{1}{f}\phi''-\left(\frac{f'}{f^2}\right)'\phi=-f\left[\frac{\phi''}{f^2}+\left(\frac{9}{8E_0}\left[\left(\frac{w'(x)}{w(x)}\right)^2\right]''+\left(\frac{9}{8E_0}\right)^2\frac{\left(\left[\left(\frac{w'(x)}{w(x)}\right)^2\right]'\right)^2}{\left(1-\frac{9}{4E_0}\left(\frac{w'(x)}{w(x)}\right)^2\right)}\right)\right]\phi\\
&=-f\left[\frac{\phi''}{f^2}+\left(\frac{9}{8E_0}\left[\left(\frac{w'(x)}{w(x)}\right)^2\right]''+\left(\frac{9}{4E_0}\right)^2\frac{\left(\frac{w'(x)}{w(x)}\frac{w''(x)}{w(x)}-\left(\frac{w'(x)}{w(x)}\right)^3\right)^2}{\left(1-\frac{9}{4E_0}\left(\frac{w'(x)}{w(x)}\right)^2\right)}\right)\right]\phi
\end{aligned} \tag{C6}$$

where

$$\left(\frac{f}{f^2}'\right)'=-\frac{1}{2}\left(\frac{\left[1-\frac{9}{4E_0}\left(\frac{w'(x)}{w(x)}\right)^2\right]'}{\sqrt{1-\frac{9}{4E_0}\left(\frac{w'(x)}{w(x)}\right)^2}}\right)'=-\frac{1}{2}\frac{\left[1-\frac{9}{4E_0}\left(\frac{w'(x)}{w(x)}\right)^2\right]''}{\sqrt{1-\frac{9}{4E_0}\left(\frac{w'(x)}{w(x)}\right)^2}}+\frac{1}{4}\frac{\left[\frac{9}{4E_0}\left(\frac{w'(x)}{w(x)}\right)^2\right]'\left[\frac{9}{4E_0}\left(\frac{w'(x)}{w(x)}\right)^2\right]'}{\left(1-\frac{9}{4E_0}\left(\frac{w'(x)}{w(x)}\right)^2\right)^{3/2}}$$

$$\left[\left(\frac{w'(x)}{w(x)}\right)^2\right]''=2\left[\left(\frac{w''(x)}{w(x)}\right)^2-5\left(\frac{w'(x)}{w(x)}\right)^2\left(\frac{w''(x)}{w(x)}\right)+\left(\frac{w'(x)}{w(x)}\frac{w'''(x)}{w(x)}\right)+3\left(\frac{w'(x)}{w(x)}\right)^4\right]$$

Finally

$$\begin{aligned}
-\frac{1}{f}\frac{d}{dx}\left[1-\frac{9}{4E_0}\left(\frac{w'(x)}{w(x)}\right)^2\right]\frac{d}{dx}f\phi=&\\
=-\frac{\phi''}{f^2}-\frac{9}{4E_0}&\left[\left(\frac{w''(x)}{w(x)}\right)^2-5\left(\frac{w'(x)}{w(x)}\right)^2\left(\frac{w''(x)}{w(x)}\right)+\left(\frac{w'(x)}{w(x)}\frac{w'''(x)}{w(x)}\right)+3\left(\frac{w'(x)}{w(x)}\right)^4\right]\phi-\\
&-\left(\frac{9}{4E_0}\right)^2\frac{\left(\frac{w'(x)}{w(x)}\frac{w''(x)}{w(x)}-\left(\frac{w'(x)}{w(x)}\right)^3\right)^2}{\left(1-\frac{9}{4E_0}\left(\frac{w'(x)}{w(x)}\right)^2\right)}\phi.
\end{aligned}$$

Substituting $\psi_0(x) = f(x)\,\phi(x)$ into the equation (31) and dividing by f gives the eigenvalue equation for ϕ:

$$E\phi = \left[-\left(1 - \frac{9}{4E_0}\left(\frac{w'(x)}{w(x)}\right)^2\right)\frac{d^2}{dx^2} + \frac{\pi^2}{w^2(x)} + \frac{\pi^2+3}{12}\left(\frac{w'(x)}{w(x)}\right)^2 + \right.$$
$$- \frac{9}{16E_0}\left\{\frac{13}{4}\left(\frac{w'(x)}{w(x)}\right)^4 - 2\frac{w''(x)}{w(x)}\left(\frac{w'(x)}{w(x)}\right)^2 + 3\left(\frac{w''(x)}{w(x)}\right)^2 + 2\frac{w'(x)}{w(x)}\frac{w'''(x)}{w(x)}\right\} -$$
$$\left. - \left(\frac{9}{4E_0}\right)^2 \frac{\left(\frac{w'(x)}{w(x)}\frac{w''(x)}{w(x)} - \left(\frac{w'(x)}{w(x)}\right)^3\right)^2}{\left(1 - \frac{9}{4E_0}\left(\frac{w'(x)}{w(x)}\right)^2\right)} \right]\phi. \tag{C7}$$

It is not clear whether this equation for ϕ is numerically preferable over that for ψ_0, Eq. (31). It could be so if the position dependent inverse mass happens to vanish at some points. This is because f diverges at such points, and $\phi(x) = \psi_0(x)/f(x)$ could have more regular behavior than $\psi_0(x)$ [but this is not certain, since also $\psi_0(x)$ seem to be at least finite there]. Note also that when the inverse mass vanishes, the potential term in the above equation diverges, which also an inconvenience in numerics.

APPENDIX D: GREEN'S FUNCTION IN 1D

1. General considerations

We express ψ_1 in terms of (the unknown) ψ_0 by (19)

$$\psi_1(x) = \frac{1}{E - \hat{H}_{11}}\hat{H}_{10}\psi_0(x) \equiv \hat{G}_{11}(E)\,\hat{H}_{10}\psi_0(x), \tag{D1}$$

where

$$\hat{G}_{11}(E) = \frac{1}{E - \hat{H}_{11}} \tag{D2}$$

is a Green's function for $\hat{H}_{11}$, i.e. for the second mode with all couplings to other modes neglected. In the position representation, $\hat{H}_{11}$ is given by (14) with index $m = 1$

$$\hat{H}_{11} = \left[-\frac{d^2}{dx^2} + \frac{9\pi^2}{w^2(x)} + \frac{3+9\pi^2}{12}\left(\frac{w'(x)}{w(x)}\right)^2 \right]. \tag{D3}$$

It seems a difficult task to obtain exactly the Green's function $\hat{G}_{11}(E)$ for an arbitrary width profile (probably this is doable for the constriction geometry?). Anyway, we need $\hat{G}_{11}(E)$ in the combination $\hat{H}_{01}\hat{G}_{11}(E)\,\hat{H}_{10}$, Eq. (15), which we want to use in the position representation. Generally, Green's function $G_{11}(E, x_1, x_2)$ is non-local, therefore we would have

$$\left\langle x_1 | \hat{H}_{01}\hat{G}_{11}(E)\,\hat{H}_{10} | x_2 \right\rangle = \int dx'dx''\delta(x_1 - x')\,\hat{H}_{01}(x_1)\,G_{11}(E, x', x'')\,\delta(x'' - x_2)\,\hat{H}_{10}(x_2)$$
$$= \hat{H}_{01}(x_1)\,G_{11}(E, x_1, x_2)\,\hat{H}_{10}(x_2), \tag{D4}$$

also a non-local operator, which becomes rather inconvenient, even if $G_{11}(E, x_1, x_2)$ is known.

Some possible directions to treat the Green's function are as follows:

1. Use the free-space Green's function.
2. Use the free-space Green's function with the perturbative corrections due to the potential in $\hat{H}_{11}$, i.e. $\hat{G} = \hat{G}_0 + \hat{G}_0\hat{V}_{11}\hat{G}_0$.
3. Neglect the 2^{nd} term in the potential in $\hat{H}_{11}$ and try to find the piece-wise solution for $G_{11}(E, x_1, x_2)$ for the narrow and the wide sections with some sewing between them (I have no idea how to do this in details, or see item (6) below). Due to the numerical experience with the Green's function this should be bad approximation for rather sharp geometries, where the term $\left(\frac{w'}{w}\right)^2$ affects strongly the Green's function.

4. Construct $G_{11}(E,x_1,x_2)$ numerically (the numerical test seems to show that, for the energy below the spectrum of $\hat{H}_{11}$, $G_{11}(E,x_1,x_2)$ depends mainly on the difference x_1-x_2).

5. Use the fact that we are interested in the energies E below the spectrum of $\hat{H}_{11}$, for which the Green's function can be approximated by a δ-function, as discussed below.

6. Calculate the Green's function for H_{11} in the semiclassical approximation using the identity relating Green's function in 1D to the two independent solutions with the intial conditions on the right and left ends of the system

$$G(E,x_1,x_2)=\frac{1}{W(E)}\left(y_1(x_1)\,y_2(x_2)\,\theta(x_2-x_1)+y_1(x_2)\,y_2(x_1)\,\theta(x_1-x_2)\right), \tag{D5}$$
$$y_1(0)=0,\quad y_1'(0)=1,\quad y_2(L)=0,\quad y_1'(L)=1,\quad W(E)=y_1(x)\,y_2'(x)-y_1'(x)\,y_2(x).$$

In the semiclassical approximation $y_1(x)\sim\exp\int_0^x\sqrt{V(x')-E}dx'$ and $y_2(x)\sim\exp\int_L^x\sqrt{V(x')-E}dx'$, i.e. by the exponentially growing from the respective boundaries solutions (the decaying ones, needed to satisfy the BC are ignored). Note that the Wronskian $W(E)\sim\sqrt{V(x)-E}$ becomes position dependent, which is because the semiclassical solution is an approximation. In fact, in the case of H_{11} the neglected term in the equation seems to be of the same order as the potential term, and the semiclassical approximation may be bad. Namely,

$$\frac{d^2}{dx^2}e^{\int_0^x\sqrt{V(x')-E}dx'}=\left(\frac{V'(x)}{2\sqrt{V(x)-E}}+V(x)-E\right)e^{\int_0^x\sqrt{V(x')-E}dx'}, \tag{D6}$$

where the first term in the parentheses on the r.h.s. should be small for the approximation to hold. However, for the effective potential in H_{ii} it seems to be of the same order (but not larger) as $V(x)$. Indeed, for H_{11}, we have at the width step where there is a maximum of the geometric potential $V(x)$ in H_{11}

$$V_{\max}(x)\sim\max\left[\frac{3+\pi^2(1+2m)^2}{12}\left(\frac{w'(x)}{w(x)}\right)^2\right]=\frac{3+\pi^2(1+2m)^2}{12}\left(\frac{\Delta w}{w}\frac{1}{\eta a}\right)^2,\ \text{and}\ \max V'(x)\sim\frac{1}{\eta a}V_{\max}(x)$$
$$\text{so that}\ \frac{V'(x)}{\sqrt{V(x)-E}}\sim\frac{1}{\sqrt{V_{\max}(x)}}\frac{1}{\eta a}V_{\max}(x)\approx\frac{1}{3}\left(\frac{w}{\Delta w}\right)V_{\max}(x)\approx V_{\max}(x). \tag{D7}$$

Thus, the semiclassical approximation would not be good quantitatively, but still could serve to obtain and/or understand some approximation for the Green's function.

Let us, first, consider the possibility in item (5) above, since this approximation means local $G_{11}(E,x_1,x_2)$, which greatly simplifies the problem. This indeed happens in the limit $E\to-\infty$, since

$$\lim_{E\to-\infty}G_{11}(E,x_1,x_2)=\lim_{E\to-\infty}\sum_n\frac{\psi(x_1)\,\psi^*(x_2)}{E-E_n}=-\frac{1}{|E|}\sum_n\psi(x_1)\,\psi^*(x_2)=-\frac{1}{|E|}\delta(x_1-x_2), \tag{D8}$$

which is independent of the form of $\hat{H}_{11}$, provided its spectrum is bounded from below. For a finite E this is an approximation and, also, some thought should be given to what is the factor in front of $\delta(x_1-x_2)$:

- naively, this factor could be the difference between E and the lower spectral edge of $\hat{H}_{11}$ (i.e. $E_{n=0}$), or
- this factor can also be studied by calculating $G_{11}(E,x_1,x_2)$ numerically and looking for the normalization of its integral as a function of E, or
- We can combine this approximation with the approximation of the free Green's function (for $\frac{\hbar^2}{2m}=1$)

$$G_0^{R,A}\left(E=k^2>0,x_1,x_2\right)=\mp i\frac{1}{2k}e^{\pm ik|x_1-x_2|}\to G_0\left(E=-\kappa^2<0,x_1,x_2\right)=-\frac{1}{2\kappa}e^{-\kappa|x_1-x_2|}, \tag{D9}$$

where the $\pm$ sign in the exponent $e^{\pm ik|x_1-x_2|}$ corresponds to $E\pm i\eta$, so that going to negative E either from above ($k\to i\kappa,\operatorname{Im}k>0$) or below ($\operatorname{Im}k<0$) the real axis gave the same result for $G_0^{R,A}$. The latter can now be approximated by the δ-function, since

$$G_0\left(E=-\kappa^2<0,x_1,x_2\right)=-\frac{1}{2\kappa}e^{-\kappa|x_1-x_2|}=-\frac{\kappa}{2\kappa^2}e^{-\kappa|x_1-x_2|}\approx-\frac{1}{|E|}\delta(x_1-x_2), \tag{D10}$$

in which case the prefactor is exactly the difference between E and the spectral edge.

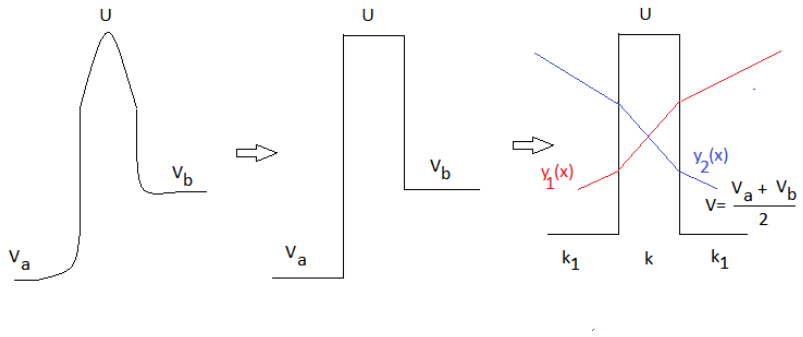

FIG. 11: Model of the geometric potential barrier used for the Green's function calculcation.

2. Constructing a non-local Green's function

The δ-function approximation for the Green's function can be made to work using some phenomenological correction of the δ-function strength. The latter depends on the smoothing parameter, and could be understood only by considering the properties of the true non-local Green's function. In fact, in the considered cases the Green's function should be considered as a non-local function, - untill the waveguide is very narrow so that the mode splitting is larger than the geometric potential peaks.

Initially, the non-local Green's function was approximated by its free space form, with the negative energy incorrectly chosen as the difference between the mean diagonal geometric potentials of the first and the second transverse modes. It turned out numerically, that the magnitude of such Green's function should have been reduces by a significant and smoothness dependent factor.

Eventually, I decided to calculate the Green's function analytically for the simplified model of the geometric potential barrier at the waveguide width steps, and to get the required coefficients from that solution. The model of the barrier is explained in Fig. 11. The original smooth profile of the barrier (a Gausian in the case of the Gaussian kernel smoothing method) is replaced by a rectangular profile. The values V_a and V_b of the potential to the left and the right of the barrier are different, but assuming high potential barrier they can be replaced by a single average value V at the last form of the approximation. It remains to fix the parametrization of the rectangular barrier in respect to the original Gaussian profile. The latter comes from the Gaussian smoothing with the kernel (64):

$$g\left(x\right)=\frac{1}{\sqrt{\pi}\eta a}e^{-\left(x/\eta a\right)^{2}},\quad\int g\left(x\right)dx=1. \tag{D11}$$

This defines the shape of the derivative of the waveguide width $w'\left(x\right)=\Delta w\times g\left(x\right)$, while the barrier part in the geometric potential is proportional to $\left(w'\left(x\right)\right)^{2}$, since for the mode m, Eq. (14),

$$V_{eff}^{(m)}\left(x\right)=\frac{\pi^{2}\left(1+2m\right)^{2}}{w^{2}\left(x\right)}+\frac{3+\pi^{2}\left(1+2m\right)^{2}}{12}\left(\frac{w'\left(x\right)}{w\left(x\right)}\right)^{2}\approx\frac{\pi^{2}\left(1+2m\right)^{2}}{w^{2}\left(x\right)}+\frac{3+\pi^{2}\left(1+2m\right)^{2}}{12}\left(\frac{\Delta w}{\bar{w}}\right)^{2}g^{2}\left(x\right), \tag{D12}$$

where the second term was approximated using the mean value of the letter width at the boundary between A and B.

$$\bar{w}\equiv\frac{w_{a}+w_{b}}{2}. \tag{D13}$$

Thus, we need to replace the unity-normalized Gaussian function $g\left(x\right)$ by a square barrier. This can be done in one of the two alternative ways:

(i) take a square barrier of the width βa and the height $\left(\beta a\right)^{-1}$, or more generally

(ii) take a square barrier of the width βa, where β is related to η due to some consideration, e.g. $\beta=2\eta$ to match the actual widths, while the height is $\lambda\left(\beta a\right)^{-1}$, where the second parameter λ is to be fixed.

In both cases the parameter β or β,λ should be related to the smoothing parameter η in the kernel $g\left(x\right)$ (64) due to some consideration of equivalence of the actual and the rectangular barriers. This relation can be considered as phenomenological, but the purpose is to make it η-independent (this is the main goal). Let us try to derive some criterion for relating β to η, while sticking to the possibility (i) above. Then, let us try the following two criteria:

(A) **Requiring same mean imaginary momentum**. We take energy $E \approx 0$, i.e. assume that the barrier height U is very large compared to E. Then the imaginary momentum is just the square root of the potential (D12), in which the first term can also be ignored for sharp enough structures. The definition of the "mean" is not definite, however, for a smooth profile like $g(x)$. It can be defined by the "importance" weighting with the potential profile itself or, alternatively, with $g(x)$. The later is already normalized to unity. Therefore, choosing $g(x)$ as a weight function up to the common constants,

$$\langle\kappa\rangle_{Gaussian} \equiv \int \sqrt{V_{eff}^{(m)}(x)}\, g(x)\, dx \approx C \int g^2(x)\, dx = \frac{C}{\sqrt{2\pi}\eta a} \int \frac{1}{\sqrt{\pi/2}\eta a} e^{-2(x/\eta a)^2} dx = \frac{C}{\sqrt{2\pi}\eta a}, \tag{D14}$$

$$\text{where } C = \sqrt{\frac{3+\pi^2(1+2m)^2}{12}} \frac{\Delta w}{\bar{w}}, \quad \Delta w = w_a - w_b, \quad \bar{w} = \frac{w_a + w_b}{2}. \tag{D15}$$

For the equivalent rectangular barrier

$$\langle\kappa\rangle_{rect} = \frac{C}{\beta a},$$

which yields

$$\beta = \sqrt{2\pi}\eta \approx 2.5\eta. \tag{D16}$$

Thus, the peak of the equivalent rectangular potential, $(C/\beta a)^2 = \left(C/\sqrt{2\pi}\eta a\right)^2$, is 2 times smaller than the Gaussian peak $\left(C/\sqrt{\pi}\eta a\right)^2$. (Note: the same relation is obtained requiring the equivalence of the intergals of the potential barriers [excluding the background part in (D12)]).

(B) **Requiring same mean potential**. The Gaussian barrier is averaged over the Gaussian weight. The latter normalized to unity is

$$\xi(x) = \left(\sqrt{2\pi}\eta a\right) g^2(x) = \frac{\sqrt{2}}{\sqrt{\pi}\eta a} e^{-2(x/\eta a)^2}, \tag{D17}$$

so that the mean barrier potential is (discarding the background level)

$$\langle V\rangle_{Gauss} = \int V_{eff}^{(m)}(x)\, \xi(x)\, dx \approx C^2 \int g^2(x)\, \xi(x)\, dx = \frac{C^2}{\sqrt{2}\pi(\eta a)^2} \int \frac{2}{\sqrt{\pi}\eta a} e^{-4(x/\eta a)^2} dx = \frac{C^2}{\sqrt{2}\pi(\eta a)^2}, \tag{D18}$$

while for the rectangular barrier

$$\langle V\rangle_{rect} = \frac{C^2}{(\beta a)^2}, \tag{D19}$$

so that the equivalence means

$$\beta = 2^{1/4}\sqrt{\pi}\eta, \tag{D20}$$

which is by $2^{1/4}$ smaller than the first estimation (D16). Correspondingly, the peak of the equivalent rectangular potential, $(C/\beta a)^2 = \left(C/2^{1/4}\sqrt{\pi}\eta a\right)^2$, is now $\sqrt{2}$ times smaller than the Gaussian peak $\left(C/\sqrt{\pi}\eta a\right)^2$.

Relations (**??**) and (D20) give a refference range for β, which finally is still could need some slight corection/adjusment due to the numerical results.

Having chosen the form of the barrier, one can find the Green's function using its expression (D5) for 1D in terms of the two independent solutions of the initial value problem for corresponding differential equation. Formally, the initial conditions for $y_1(x)$ and $y_2(x)$ should fit the boundary conditions for G on the left and the right side respectively (e.g. zero BC for the finite line, or non-diverging BC for the infinite line). We have a finite system, but it is evident that essentially the same Green's function would be obtained in the infinite system with a similar local structure. Thus, we need actually two solutions $y_1(x)$ and $y_2(x)$ decaying to the left and to the right respectively (see Fig. 11). Moreover, we do not need to find the large scale solution, but only its form in the region of the interest, which is only the under-barrier interval for both x_1 and x_2 in $G(x_1, x_2, E)$. This follows from the specific combination in which the Green's function is used, namely $\hat{H}_{01}\hat{G}_{11}(E)\,\hat{H}_{10}$, Eq. (21). Since the width of $G(x_1, x_2, E)$ is much smaller than

the letter length, it "connects" only structures in $\hat{H}_{01}$ and $\hat{H}_{10}$ which originate from the same width step. These structures are practically confined to the spatial region under the geometric potential barrier, and vanish fast outside it (see (28,29)). Thus, indeed, we need to know $G(x_1, x_2, E)$ only under the barrier.

Let us find the solutions $y_1(x)$ and $y_2(x)$ assuming formally an single rectangular barrier of the height U in $x \in [0, x_0]$ over the background V, Fig. 11. Recall that energy E is below the potential V, so that we have only the imaginary momentum

$$k_1 = (V - E)^{1/2}, k = (U - E)^{1/2} \tag{D21}$$

We take the growing form $y_1(x) = e^{k_1 x}$ for $x < 0$ and $y_1(x) = Ae^{-kx} + Be^{kx}$ under the barrier [and we are not interested in $y_1(x > x_0)$]. Matching the solutions gives

$$\begin{cases} 1 = A + B \\ k_1 = -kA + B \end{cases} \rightarrow \begin{cases} A = \frac{k - k_1}{2k} \\ B = \frac{k + k_1}{2k} \end{cases} . \tag{D22}$$

Solution $y_2(x)$ is found symmetrically to $y_1(x)$, and finally

$$y_1(x) = \begin{bmatrix} e^{k_1 x} & x < 0 \\ Ae^{-kx} + Be^{kx} & 0 \le x \le x_0 \end{bmatrix}, \quad y_2(x) = \begin{bmatrix} e^{-k_1(x - x_0)} & x < 0 \\ Ae^{-kx_0}e^{kx} + Be^{kx_0}e^{-kx} & 0 \le x \le x_0 \end{bmatrix} . \tag{D23}$$

The Wronskian (which is indpendent of the position) is

$$W(E) = -\left[y_1'(x) y_2(x) - y_1(x) y_2'(x)\right]_{x=0} \tag{D24}$$

$$= -k_1\left(Ae^{-kx_0} + Be^{kx_0}\right) + k\left(Ae^{-kx_0} - Be^{kx_0}\right) = -\frac{(k_1 + k)^2}{2k}e^{kx_0} + \frac{(k_1 - k)^2}{2k}e^{-kx_0}. \tag{D25}$$

To simlify even further, we assume

$$k \gg k_1, \tag{D26}$$

which is reasonable for sharp width variation (but with some adjustment works also for rather smooth structures, - see below). Then, the expressions simplify further for $0 \le x \le x_0$:

$$\begin{bmatrix} y_1(x) = \cosh kx \\ y_2(x) = \cosh k(x - x_0) \\ W(E) = -k \sinh kx_0 \end{bmatrix}, \quad 0 \le x \le x_0 \tag{D27}$$

Finally the Green's function in $0 \le x_1, x_2 \le x_0$ is

$$G(x_1, x_2, E) = \frac{y_1(x_1) y_2(x_2)}{W(E)} = -\frac{\cosh(kx_1)\cosh k(x_2 - x_0)}{k \sinh kx_0}, \quad 0 \le x_1, x_2 \le x_0, \tag{D28}$$

which (in a sense) is symmetric with respect to the middle of the barrier (but asymmetric for any given fixed $x_1$or x_2).

As expected, $G(x_1, x_2, E)$ in (D28) is not translationally invariant. Therefore, as a further approximation, we want to find some equivalent average Green's function for $x_1, x_2 \in [0, x_0]$, which would be translation invariant. This is in order to be able to realize the action of the Green's function as a plain convolution with a position-independent kernel. To do so, the Green's function in (D28) should be averaged in a certain way and, then, related to the symmetric exponential equivalent. The above procedure can, actually, be done in different ways to yield somewhat different results. The following method was chosen. To do the average, x_1 in (D28) is written as $x_1 = x_2 - y$, $y > 0$, and the obtained expression averaged over $x_2 \in [y, x_0]$ at a fixed y. This gives

$$\langle G(x_2 - y, x_2, E)\rangle_{x_2 \in [y, x_0]} = -\frac{1}{2k \sinh kx_0}\left[\cosh k(x_0 - y) + \frac{\sinh k(x_0 - y)}{k(x_0 - y)}\right], \tag{D29}$$

which yields values of the peak and the derivative at the peak (i.e. for $y \to 0$):

$$\langle G(x_2, x_2, E)\rangle_{x_2 \in [0, x_0]} = -\frac{1}{2k \sinh kx_0}\left[\cosh kx_0 + \frac{\sinh kx_0}{kx_0}\right], \tag{D30}$$

$$\frac{d}{dx_1}\langle G(x_1, x_2, E)\rangle_{x_2 \in [0, x_0], (x_1 = x_2)} = -\frac{k}{2k \sinh kx_0}\left[\sinh kx_0 + \frac{kx_0 \cosh kx_0 - \sinh kx_0}{(kx_0)^2}\right]. \tag{D31}$$

Thus, if the average Green's function is to be substituted with a simple two-sided exponential $\tilde{G}(x_1, x_2, E)$ fitting these two values, then

$$\langle G(x_1, x_2, E)\rangle \Leftrightarrow \tilde{G}(x_1, x_2, E) = -\frac{1}{2k\sinh kx_0}\left[\cosh kx_0 + \frac{\sinh kx_0}{kx_0}\right] e^{-\kappa|x_2-x_1|}, \tag{D32}$$

where the exponent

$$\kappa = k\frac{(kx_0)^2\sinh kx_0 + kx_0\cosh kx_0 - \sinh kx_0}{(kx_0)(kx_0\cosh kx_0 + \sinh kx_0)} \tag{D33}$$

is set to match the value of the derivative at the peak of the Green's function[2]. In the limit $k \to \infty$, one obtains the free particle result

$$\tilde{G}(x_1, x_2, E) = -\frac{1}{2k}e^{-k|x_2-x_1|}. \tag{D37}$$

With the chosen equivalent Green's function $\tilde{G}(x_1, x_2, E)$, Eq. (D32), it remains to determine explicitly the parameters k and x_0. In this document and in the numerical routines the units are chosen so that $\frac{\hbar^2}{2m} = 1$, therefore the imaginary momentum k is given by

$$k^2 = V_{eff}^{(m)} - E, \tag{D38}$$

where we set E to the ground state of the lowest ($m = 0$) mode, estimating it as

$$E = \frac{\pi^2}{w_a^2}$$

Taking into account the smoothing, the backbround term in (D12) for the considered mode $m = 1$ can be evaluated at $w = \bar{w} = \frac{w_a+w_b}{2}$ while the second term in $V_{eff}^{(m)}$ (D12) is determined by the height of the equivalent rectangular barrier. Therefore

$$k = \left[\frac{\pi^2(1+2m)^2}{\bar{w}^2} + \frac{3+\pi^2(1+2m)^2}{12}\left(\frac{\Delta w}{\bar{w}}\frac{1}{\beta a}\right)^2 - \frac{\pi^2}{w_a^2}\right]^{1/2} \tag{D39}$$

$$= \left[4(1+2m)^2\left(\frac{a}{\bar{w}}\right)^2 + \frac{3+\pi^2(1+2m)^2}{3\pi^2}\left(\frac{\Delta w}{\bar{w}}\frac{1}{\beta}\right)^2 - 4\left(\frac{a}{w_a}\right)^2\right]^{1/2} E_r^{1/2}, \tag{D40}$$

where in the second line the recoil energy $E_r = \frac{\pi^2}{4a^2}$ was used, and $m = 1$ for the second mode. The remaining parameter x_0 is just the width of the equivalent rectangular barrier, so that

$$x_0 = \beta a, \tag{D41}$$

whereas β is related to the smoothness parameter η by Eqs. (D16,D20). The latter do not coincide and define a range of possible values for β. Numerically, the proper results were obtained for β given by (D20), i.e.

$$\beta = 2^{1/4}\sqrt{\pi}\eta. \tag{D42}$$

---

[2] **Note:** it is interesting to note that for any, e.g., $x_2 \in [0, x_0]$ the left and right slopes of $G(x_1, x_2, E)$ at the peak $x_1 = x_2$,

$$\frac{d}{dx_1}G(x_1, x_2, E) = \frac{1}{k\sinh kx_0}\left[k\sinh(kx_1)\cosh k(x_0 - x_2)\right]_{x_1=x_2}, \tag{D34}$$

$$\frac{d}{dx_2}G(x_1, x_2, E) = -\frac{1}{k\sinh kx_0}\left[k\cosh(kx_1)\sinh k(x_0 - x_2)\right]_{x_1=x_2}, \tag{D35}$$

are different, but average of their absolute values is constant

$$\frac{1}{2}\left[\frac{d}{dx_1}G(x_1, x_2, E) - \frac{d}{dx_2}G(x_1, x_2, E)\right]_{x_1=x_2} = \frac{1}{k\sinh kx_0}\frac{k}{2}\sinh kx_0 = \frac{1}{2}. \tag{D36}$$

Example: let's note that for a sharp structure, the derivative term in $V_{eff}^{(m)}$ is dominant, therefore

$$kx_0 \approx \sqrt{\frac{3+\pi^2\left(1+2m\right)^2}{12}}\left(\frac{\Delta w}{\bar{w}}\frac{1}{\beta a}\right)\beta a = \sqrt{\frac{3+\pi^2\left(1+2m\right)^2}{12}}\frac{\Delta w}{\bar{w}}, \tag{D43}$$

which gives $kx_0 \approx 1.46$ for $m=1$, $\Delta w = 1.5\,\mu$m and $\bar{w} = 2.7\,\mu$m. Then

$$\kappa = 0.72k, \quad \tilde{G}\left(x_1, x_2, E\right) = \frac{1.3}{2\kappa}e^{-\kappa|x_2-x_1|} \tag{D44}$$

3. Numerical results for the Green's function in Fibonacci wire

sdf

APPENDIX E: NOTES AN NUMERICAL SOLUTION OF THE SCATTERING PROBLEM

Scattering problem is solved as a Cauchy problem with an outgoing boundary conditions set on the transmission side (in 1D). Our effective 1D Schrodinger equation contains a position dependent mass. Although it seems that the latter would not vanish in practice, it is worthy of applying the numerical solution scheme immune to the case of the vanishing mass. The differential term of the form

$$\frac{d}{dx}Q\left(x\right)\frac{d}{dx}f\left(x\right) \tag{E1}$$

can be discretized in different ways, one of which is as follows

$$\left[\frac{d}{dx}Qf'\right]_{n+1} = \left[Qf'\right]_{n+1} - \left[Qf'\right]_n = Q_{n+1}f'_{n+1} - Q_nf'_n = Q_{n+1}\left(f_{n+1}-f_n\right) - Q_n\left(f_n - f_{n-1}\right). \tag{E2}$$

The (simplest) numerical scheme would express f_{n+1} in terms of the values on the previous grid points. If there is a possibility that $Q_{n+1}=0$, then it should be examined numerically, and the "dangerous" point be circumvented. One way to do this is "jumping" over that particular point by, e.g. doubling the grid spacing at the corresponding iteration. Another possibility is to use

$$\frac{d}{dx}Q\left(x\right)\frac{d}{dx}f\left(x\right) = Q'\left(x\right)f'\left(x\right) + Q\left(x\right)f''\left(x\right), \tag{E3}$$

where *near* the point $Q\left(x\right)=0$ (i.e. when $|Q\left(x\right)|$ is small, - not only at the node point) the term with $f''\left(x\right)$ would be ignored, and the numerical scheme proceeds with

$$\frac{d}{dx}Q\left(x\right)\frac{d}{dx}f\left(x\right) \approx Q'\left(x\right)f'\left(x\right) \to Q'_{n+1}\left(x\right)f'_{n+1} = \left(Q_{n+1}-Q_n\right)\left(f_{n+1}-f_n\right). \tag{E4}$$

Now, it is highly non-probable that coefficient of f_{n+1} would vanish simultaneously in (E2) and (E4) [i.e. $Q\left(x\right)$ and its derivative vanish simultaneously].

Note some alternative numerical discretization schemes:

$$\begin{aligned}\left[\frac{d}{dx}Q\left(x\right)\frac{d}{dx}f\left(x\right)\right]_{n+1} &= \left[Q'\left(x\right)f'\left(x\right)\right]_{n+1} + \left[Q\left(x\right)f''\left(x\right)\right]_{n+1} \\ &= \left(Q_{n+1}-Q_n\right)\left(f_{n+1}-f_n\right) + Q_{n+1}\left(f_{n+1}-2f_n+f_{n-1}\right),\end{aligned} \tag{E5}$$

or slightly different one

$$\begin{aligned}\left[\frac{d}{dx}Q\left(x\right)\frac{d}{dx}f\left(x\right)\right]_{n+1} &= \left[Q'\left(x\right)f'\left(x\right)\right]_{n+1} + \left[Q\left(x\right)f''\left(x\right)\right]_{n+1} \\ &= \left(Q_{n+1}-Q_n\right)\left(f_{n+1}-f_n\right) + Q_{n+1}\left(f_{n+2}-2f_{n+1}+f_n\right).\end{aligned} \tag{E6}$$

APPENDIX F: WIRES 18 AND 15

This new system has different parameters (as provided by Dimitrii in the files "Overviewdata2324_1_2014_2.pptx" and "Wire15.pptx"):

$$\text{Wire 18: } w_a = 3.5\,\mu\text{m}, w_b = 1.86\,\mu\text{m}, a = 0.8\,\mu\text{m}, E_x = 1605\,\text{meV}, \delta_0 = -8.3\,\text{meV}, \tag{F1}$$

$$\text{Wire 15: } w_a = 3.5\,\mu\text{m}, w_b = 1.86\,\mu\text{m}, a = 0.5\,\mu\text{m}, E_x = 1607\,\text{meV}, \delta_0 = -8.7\,\text{meV}, \tag{F2}$$

and it is a pure S_{13} system with 233 letters without any paddings. Some new calculcations for this system should be done with slightly different settings.

Numerical facts tested on shorter S_{10} (54 letters) to examine the convergence for the Wire_18 (the geometry is important here, not the ex-phot coupling):

1. For the relative smoothness $0.2 \times (1.35/0.8) \times 1.07/8$, there is some noticible difference between the 2-mode versus 3-mode calculcation, expressed in the band edge shifts of about 0.15 meV. The corresponding difference between 3-mode and 4-mode calculations is about 0.01 meV, i.e. negligible.

2. Since the letter is about twice shorter than before, the parameter $P_{grating}$ can taken about twice smaller, i.e. about 80 for the above smoothness, - if not to high longitudinal modes are included.

3. The number of states per mode 5×400 seems to be enough for the above smoothness in S_{10} (54 letters) [for longer system it should be increased proportionally] as long as the first two and the lower part of the third "main" subbands are concerned. At higher energies it seems to be marginal, probably because of the vicinity to the 2nd mode.

4. Using stronger smoothness one can do lower resolution calculcation (less transverse and longitudinal modes) and still recover the higher resolution one for sharper structure. In the considered case, 2-mode with 3×400 states (convergent to 5×400) for the smoothness $0.5 \times (1.35/0.8) \times 1.07/8$ reproduces the above result ($0.2 \times (1.35/0.8) \times 1.07/8$) for 3-mode with 5×400 states calculation (virtually exact for the first two main band, and rather close up to ~ 0.05 meV for the third one). Similarly, 1-mode calculcation with 3×400 states for the smoothness $2 \times (1.35/0.8) \times 1.07/8$ reproduces the 1st band, rather closely the $2nd$ one but less good (up to $0.1 - 0.2$ meV) the 3rd one. Note that this smoothness is an exaggeration, but the physical counterpart is $0.2 \times (1.35/0.8) \times 1.07/8$ which is reasonable (judging due to the micrographs).

5. For the smoothness $0.1 \times (1.35/0.8) \times 1.07/8$, convergence is mode difficult. Calc using 3 modes and $P = 160$, for 3×400 states is very different from that for 5×400 states, which is still noticable different from that for 6×400 states. The latter is same (in the 1st two main bands and the beginning of the 3rd one) as for the smoothness $0.2 \times (1.35/0.8) \times 1.07/8$ with 3 modes and $P = 160$, for 3×400, but for higher energy goes like the convergent calculation for that smoothness.

Wire_18

The final calculation for the system "Wire_18" S_{13} (233 letters) with the above parameters was done using the smoothing parameter $2 \times (1.35/0.8) \times 1.07/8$ for 1D calculation (NO coupling correction) with 4×400 states and $P = 80$, or $0.5 \times (1.35/0.8) \times 1.07/8$ for 2D calculation with 8×400 states and $P = 40$ [which both are equivalent to the convergent 2D with smoothness $0.2 \times (1.35/0.8) \times 1.07/8$].

Additionally, 2D calculcation was done as above but with the refractive index changed from 3.25 to 3.33, which squizes the energy scale by ~ 1.05. This seems to improve the agreement with the experiment (especially the lower edge of the 3rd band the position of structure at 1598 meV, and seems to satisfy Dimitrii (by 31/01/2014). Besides, similar calculation with former $n = 3.25$, but smoothness $0.3 \times (1.35/0.8) \times 1.07/8$ was done (data saved in MET file), to smulate physical smoothness above $0.2 \times ....$ The band and gaps are shifted to the right, whivh could only be corrected with still higher n than 3.33.

Wire_15

The 1D calculation seems to fail **finally** for any reasonable smoothness. The "light" 2D calculation seems to do some work using smoothness $1.5 * (1.35/0.5) * 1.07/8$, 6×400 states and $P = 40$ (MATLAB limitations for S_{13}).

Convergence: 3-mode calculation: S_{10} for $0.2 \times (1.35/0.8) \times 1.07/8$, $[5 \times 400\ (P = 160 \Leftrightarrow P = 80)] \Leftrightarrow 3 \times 400(\ P = 40)$, and it is nearly the same as $2 \times 400(\ P = 40)$ [some slight blue-shift above $E = 1598.5$]. 2-mode calculation $3 \times 400\ (\ P = 80) \Leftrightarrow 2 \times 400(\ P = 80)$, similar to 3-mode but blue-shift $\sim 0.1 - 0.15$ meV above $E = 1598.5$ meV. Increasing smoothness to $0.5 - 0.6$ makes 2-mode calculation rather similar to 3-mode one except above $E = 1600.5$ meV. The 2-mode result does not change when going to $P = 40$ (for same smoothness).

Fitting the experiment: 2-mode calculation is done for S_{13} (233 letters) using 8×400 states and $P = 40$. Then, the 2-mode result for $Sm = 0.15$ gives to large gaps: twice too big gap at 1596, but same wrong position $(1598 - 99)$ of the 2nd gap at $1599 - 1600$. Results for $Sm = 0.3 \times ...$ and $Sm = 0.5 \times ...$ seems to be optimal. Both data a saved. Finally, the latter one was chosen for the paper (meanwhile).

---

[1] D. Tanese *et. al.*, *"Polariton condensation in solitonic gap states in a 1D periodic potential"*, Nature Comm. 4, 1749 (2013), DOI: 10.1038/ncomms2760

[2] Giovanna Panzarini and Lucio Claudio Andreani, Phys. Rev. B **60**, 16799 (1999).

[3] P. Leboeuf and N. Pavloff, "Bose-Einstein beams: Coherent propagation through a guide", ??? (2001).

[4] S. Schwartz *et. al.*,"One-dimensional description of a Bose–Einstein condensate in a rotating closed-loop waveguide", New J. of Physics **8, 162** (2006).

[5] H. S. Nguyen *et. al.*, "Realization of a Double-Barrier Resonant Tunneling Diode for Cavity Polaritons", Phys.Rev.Lett. **110**, 236601 (2013).